

Fractal Modeling of Natural Terrain: Analysis and Surface Reconstruction with Range Data

KENICHI ARAKAWA¹ AND ERIC KROTKOV

School of Computer Science, Carnegie Mellon University, Pittsburgh, Pennsylvania 15213

Received July 10, 1995; revised June 3, 1996; accepted June 17, 1996

In this paper we address two issues in modeling natural terrain using fractal geometry: estimation of fractal dimension, and fractal surface reconstruction. For estimation of fractal dimension, we extend the fractal Brownian function approach to accommodate irregularly sampled data, and we develop methods for segmenting sets of points exhibiting self-similarity over only certain scales. For fractal surface reconstruction, we extend Szeliski's regularization with fractal priors method to use a temperature parameter that depends on fractal dimension. We demonstrate both estimation and reconstruction with noisy range imagery of natural terrain. © 1996 Academic Press, Inc.

1. INTRODUCTION

Many problems in the analysis of natural surface shapes and the construction of terrain maps to model them remain unsolved. One reason is that the familiar Euclidean geometry of regular shapes, such as surfaces of revolution, does not capture well the irregular and less structured shapes found in nature, such as a boulder field or surf washing onto a beach.

Mandelbrot [20-22] proposed fractals as a family of mathematical functions to describe natural phenomena such as coastlines, mountains, branching patterns of trees and rivers, clouds, and earthquakes. Since Mandelbrot introduced them, fractal sets and functions have been found to describe many other environmental properties [7], and have received a great deal of attention from scientists, artists, and others.

This paper addresses two issues in fractal modeling (Fig. 1):

1. Estimating the fractal dimension of natural surfaces given range data. Such estimates are descriptors of natural terrain that express its roughness. These estimates are valuable for such purposes as mobile robot path planning around rough terrain, compression of terrain maps, and geological analysis of terrain morphology.

2. Reconstructing natural surfaces, given sparse range data and the fractal dimension. Surface reconstruction provides knowledge of surface geometry that is valuable for such purposes as mobile robot obstacle avoidance, decomposition of terrain data, and realistic terrain visualization.

The first issue has been explored by a number of authors, who have given algorithms for estimating fractal dimension. In this paper, we extend that work to the case of natural terrain patterns acquired by a laser rangefinder. This extension requires handling fairly noisy depth data, and handling points that are not spaced regularly over the terrain.

The need to handle irregularly spaced data derives from laser rangefinders and camera-based computer vision systems, which typically acquire depth data in a sensor-centered spherical coordinate system. As one would expect, regularly spaced samples in the spherical system map onto irregularly spaced samples in a Cartesian system. Figure 2 illustrates how, in a Cartesian system, a sensor (either camera or rangefinder) acquires denser range data from closer objects, and sparser range data from farther objects, despite a regular sampling in the image.

The second issue has not received much attention. In this paper, we define the *natural surface reconstruction problem* of constructing dense elevation maps of natural surfaces, given sparse and irregularly spaced depth data. This problem differs from the traditional surface reconstruction problem in requiring that the reconstructed surface realistically reflect the rough, original surface. In contrast to approaches to surface reconstruction that impose smoothness constraints, our approach to natural surface reconstruction imposes *roughness constraints*.

A problem related to the second issue is to compute the uncertainty on the reconstructed surface. We have developed and demonstrated a Monte Carlo algorithm for computing this uncertainty [2], but will not present it in this paper since it does not directly concern fractal modeling.

This paper is organized as follows. In Section 2, we present an extension to existing fractal dimension estimation algorithms, enabling them to cope with irregularly

¹ Current address: NTT Human Interface Labs, 3-9-11 Midori-cho, Musashino-shi, Tokyo 180 Japan. E-mail: arakawa@nttarm.ntt.jp.hil.

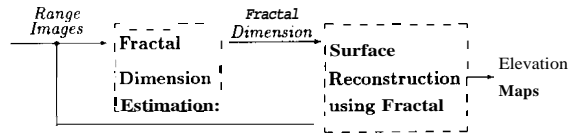


FIG. 1. Approach to modeling natural terrain based on fractal geometry.

spaced data. In Section 3, we present a surface reconstruction technique that computes elevation maps at arbitrary resolution, yet preserves the roughness of the original pattern. In the final section, we summarize the findings and identify directions for future research.

2. ESTIMATING FRACTAL DIMENSION

In this section, we first review related research. Next, we define formally some terms related to self-similarity and self-affinity. With these definitions in hand, we then describe the fractal Brownian function approach, and present results of experiments with synthetic patterns. Finally, we extend the approach to handle irregularly spaced data, and present results for range images.

2.1. Related Research

Several classes of techniques for estimating fractal dimension have been reported in the literature: box-counting, ϵ -blanket, spectral analysis, and fractal Brownian function approaches.

The box-counting approach counts the number of boxes of various sizes which cover a fractal pattern [36]. One shortcoming of this approach was identified (and circumvented) by Keller *et al.* [15], who report that the fractal dimension estimated by such methods saturates as it approaches 3.0.

The ϵ -blanket method was proposed by Peleg *et al.* [25] as a variation on the box-counting approach, and they applied the method to classification of natural textures. The method has been explored by Dubuc [10], and Dubuc *et al.* [11] for estimating the fractal dimension of both curves and surfaces.

As suggested by Mandelbrot [21], if the target pattern is assumed to be generated under the fractional Brownian motion model, spectral analysis methods [16, 26] can be applied to estimate the fractal dimension. These methods estimate the fractal dimension by linear regression on the log of the observed power spectrum as a function of the frequency. Wornell [37] proposed a representation of $1/f$ processes using orthogonal wavelet bases, and applied it to various one-dimensional signal processing tasks, including estimating fractal dimension with the maximum likelihood approach.

Other approaches that do not fit comfortably in the above categories have been developed. For example, Maragos and Sun [23] use morphological operations with varying structuring elements to evaluate the fractal dimension, and develop an iterative optimization method that converges to the true fractal dimension.

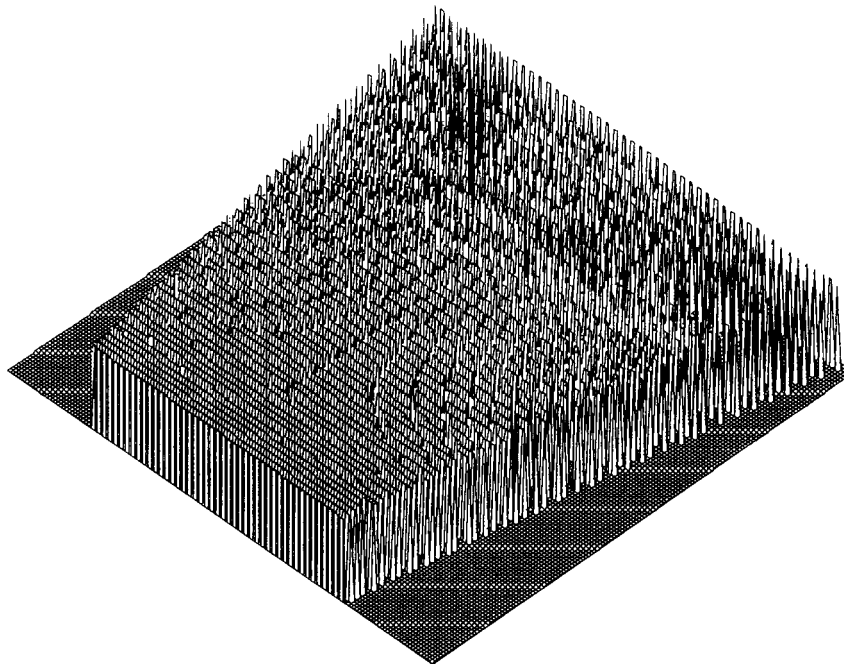


FIG. 2. Typical sampling pattern for rangefinder or camera. This figure shows the elevations in a Cartesian system when a scanning rangefinder observes a horizontal plane. The sensor acquires denser range data from closer objects, and sparser range data from farther objects.

All of these estimation methods apply to regularly sampled patterns, such as images. They do not apply to irregularly sampled patterns, such as terrain maps constructed from range data. Lundahl *et al.* [19] and Deriche and Tewfik [9] developed methods to estimate fractal dimension based on computing a maximum likelihood estimate of the autocorrelation matrix of discrete fractional Gaussian noise, which is a discrete version of the changes of fractional Brownian motion. These methods were demonstrated with regularly sampled one-dimensional signals. In principle, these methods could be applied to irregularly sampled signals also, although at significant computational expense. With regularly sampled data, the autocorrelation matrix is positive, symmetric, and Toeplitz. Thus, it is relatively easy to compute the inverse and the determinant necessary to compute the likelihood function. In the case of irregularly sampled data, the autocorrelation matrix is no longer Toeplitz, so inverting the matrix requires significant computational effort.

The maximum likelihood methods apply well to one-dimensional signals, because the rows and columns of the autocorrelation matrix correspond to the differences of signal values. Indeed, Lundahl *et al.* [19] applied the method to profiles of an image and estimated fractal dimensions of one-dimensional profile signals in various directions independently. However, the generalization to two-dimensional isotropic signals does not appear to have been published.

Unlike all the methods above, the fractal Brownian function approach does apply to irregular sampling, because it is based on a probabilistic model on the distance between data points. This model applies no matter what the spacing of samples, so long as the number of samples is sufficient. Before describing in detail this approach in Section 2.3, we define formally several terms.

2.2. Definitions

In a Euclidean space of dimension E , consider a set S of points $\mathbf{x} = (x_1, \dots, x_E)$. After scaling by r , $0 < r$, the set S becomes rS , with points $r\mathbf{x} = (rx_1, \dots, rx_E)$.

The set S is *self-similar* when S is the union of N distinct (nonoverlapping) subsets, each of which is identical, up to translation and rotation, to rS . The fractal dimension D of self-similar S then satisfies

$$1 = Nr^D \quad \text{or} \quad D = -\log N / \log r. \quad (1)$$

The set S is *statistically self-similar* if it is composed of N distinct subsets, each of which is scaled by ratio r from the original, and is identical in all statistical respects to rS . The fractal dimension of statistically self-similar S is given by (1).

A collection of real scaling factors $\mathbf{r} = (r_1, \dots, r_E)$, with

$r_j > 0$, determines an *affinity* Ψ , where Ψ transforms $\mathbf{x} \in S$ into $\Psi(\mathbf{x}) = (r_1x_1, \dots, r_Ex_E)$. This operation transforms S into $\Psi(S)$ by scaling different coordinates by different amounts. The set S is *self-affine* when S is the union of N distinct subsets, each of which is identical to the sets transformed by affine Ψ . If the condition of invariance under nonuniform scaling is satisfied statistically, the set is *statistically self-affine* (cf. the definition of statistical self-similarity).

In (1) we defined fractal dimension in terms of the self-similar set S . We can also define it in terms of the self-affine set S [36], but for the purposes of this paper, we will define it in terms of one particular class of self-affine patterns, those generated by fractional Brownian motion.

2.3. Fractal Brownian Function Approach

One class of fractal patterns is created by a process with fractional Brownian motion. The *fractal Brownian function* approach applies to this class by fractal patterns. In this section, we explain fractional Brownian motion, define fractal Brownian functions, and discuss methods proposed for using them to estimate fractal dimension.

Brownian motion $B(t)$ is a stochastic process defined as follows.

1. $B(0) = \text{constant}$.
2. $B(b) - B(a) \sim N(0, (b - a)\sigma^2)$, for $a \leq b$.

Note that $B(b) - B(a)$ and $B(c) - B(b)$ are statistically independent, for $a \leq b \leq c$.

This can be rewritten as

$$B(rt) = r^{1/2}B(t).$$

A trace of $B(t)$ requires different scaling factors in the two coordinates: r for t , but $r^{1/2}$ for $B(t)$. Therefore, it is self-affine.

Fractional Brownian motion $B_H(t)$ generalizes Brownian motion, and is defined as follows.

1. $B_H(0) = \text{constant}$.
2. For constant C ,

$$B_H(t) - B_H(0) = C \left[\int_0^t \{(t-s)^{H-1/2} - (-s)^{H-1/2}\} dB(s) + \int_0^t (t-s)^{H-1/2} dB(s) \right].$$

A trace of $B_H(t)$ exhibits a statistical scaling behavior. If the scale t is changed by the factor r , then the increments $\Delta B_H(t)$ change by a factor r^H :

$$\Delta B_H(rt) \propto r^H \Delta B_H(t).$$

Traces of fractional Brownian motion are one class of fractal patterns.

Pentland [26] defined a **fractal Brownian function** as an extension of statistical self-affinity that characterizes self-affine processes, including fractional Brownian motion. A random function $f(t)$ is a fractal Brownian function if, for all t and Δt , there exists H in

$$\Pr \left\{ \frac{f(t + \Delta t) - f(t)}{\Delta t^H} < x \right\} = g(x) \quad (2)$$

which is independent of Δt , where $g(x)$ is a cumulative distribution function. In this definition, $\Delta f_{\Delta t} = f(t + \Delta t) - f(t)$ is statistically self-affine, and H is a self-affinity parameter, related to the fractal dimension D of $f(t)$ by $D = 2 - H$. If $g(x)$ is a zero-mean Gaussian with unit variance, then $f(t)$ represents fractional Brownian motion $B_H(t)$. If, in addition, $H = 1/2$, then $f(t)$ represents classical Brownian motion $B(t)$.

Interpreting t as a vector quantity \mathbf{t} extends this definition to higher topological dimensions. In this case, the Δ appearing in the denominator of (2) must be rewritten as the norm $\|\Delta \mathbf{t}\|$. If $f(\mathbf{t})$ is a pattern in D -dimensional Euclidean space, then $D = E + 1 - H$ [36]. For instance, if we analyze fractal dimension of natural terrain, we can express the terrain as an elevation map $f(\mathbf{t})$ on a horizontal plane $\mathbf{t} = (x, y)$ and the fractal dimension can be estimated by $D = 3 - H$.

Pentland [26] proves that under certain conditions (constant illumination, constant albedo, and a Lambertian surface reflectance function), a three-dimensional surface with a spatially isotropic fractal Brownian shape produces an image (i) whose intensity surface is fractal Brownian, and (ii) whose fractal dimension is identical to that of the components of the surface normal. He also shows that the definition of a fractal Brownian function on intensity $I(\mathbf{t})$ —instead of $f(t)$ in (2)—can be rewritten as

$$E(\Delta I_{\|\Delta \mathbf{t}\|}) \|\Delta \mathbf{t}\|^{-H} = E(\Delta I_{\|\Delta \mathbf{t}\|=1}), \quad (3)$$

where $E(\Delta I_{\|\Delta \mathbf{t}\|})$ is the expected value of the change in intensity $I(\mathbf{t})$ over distance $\|\Delta \mathbf{t}\|$. Note that $\Delta I_{\|\Delta \mathbf{t}\|}$ is always positive.

To evaluate the suitability of this fractal model for images of natural surfaces, he observed the empirical distributions of intensity differences $\Delta I_{\|\Delta \mathbf{t}\|}$ for different distances $\|\Delta \mathbf{t}\|$. He observed the distributions to be approximately Gaussian. Moreover, he computed the standard deviation $S(\Delta I_{\|\Delta \mathbf{t}\|})$ of each distribution, and found the points $(\log \|\Delta \mathbf{t}\|, \log S(\Delta I_{\|\Delta \mathbf{t}\|}))$ to lie on a line. From this line in log-log space, he estimated the slope H , which is

$$H = \frac{\partial \log S(\Delta I_{\|\Delta \mathbf{t}\|})}{\partial \log \|\Delta \mathbf{t}\|}. \quad (4)$$

Given H , the fractal dimension of the two-dimensional pattern is $D = 3 - H$.

Yokoya [38] also assumed that intensity in images is distributed by a fractal Brownian function, and that $g(x) = N(0, \sigma^2)$. He developed a method for estimating fractal dimension similar to Pentland's. Instead of the standard deviation in (4), he used the expected value $E(\Delta I_{\|\Delta \mathbf{t}\|})$:

$$H = \frac{\partial \log E(\Delta I_{\|\Delta \mathbf{t}\|})}{\partial \log \|\Delta \mathbf{t}\|}. \quad (5)$$

Both methods are reasonably robust against noisy data, because they use statistics computed from a large number of data points. Yokoya's method, in particular, tolerates zero-mean normally distributed sensor noise, because the method implicitly performs an averaging operation.

The computational complexity of both methods is $O(N \|\Delta \mathbf{t}_{\text{search}}\|)$ for regularly sampled data, where N is the number of data points, and $\|\Delta \mathbf{t}_{\text{search}}\|$ is the maximum search size. Because Pentland's method computes the standard deviation, it requires slightly more computation than Yokoya's method, which computes the first moment.

2.4. Estimation from Irregularly Sampled Elevation Data

In previous sections, we have discussed fractal dimension estimation from image intensity $I(\mathbf{t})$; here, we consider elevation $z(\mathbf{d})$ (with $\mathbf{d} = (x, y)$) instead of $I(\mathbf{t})$. The procedure for estimating fractal dimension from a set of irregularly sampled elevations $z(\mathbf{d})$ is stated in the following three steps.

1. Compute statistics of $|z_{x,y} - z_{x+dx, y+dy}|$.

In the sensor frame, consider two points on the xy plane: (x, y) and $(x + dx, y + dy)$. The Euclidean distance between them is $\Delta \mathbf{d} = \sqrt{dx^2 + dy^2}$. We are interested in statistical variations in the absolute value of the difference in elevation between these two points: $\Delta z_{\Delta \mathbf{d}} = |z_{x,y} - z_{x+dx, y+dy}|$. Pentland's method requires the standard deviation of the distribution of elevation differences; Yokoya's method requires the expected value of the distribution of elevation differences.

Because the data points are distributed irregularly on the xy plane in the sensor frame, we must extend the original methods, which assume the data is distributed regularly, or equivalently, that the sampling interval is constant. For $i = 0, 1, \dots, m$, and $\Delta \mathbf{d}_i < \Delta \mathbf{d}_{i+1}$, we prepare counters A_i , B_i , and C_i to correspond to distance $\Delta \mathbf{d}_i$. These counters are for computing expected values, standard deviations, and numbers of sample pairs, respectively. Let ϵ be a small distance that satisfies $0 < \epsilon < \Delta \mathbf{d}_i$ for any i . This parameter represents the width of a circular

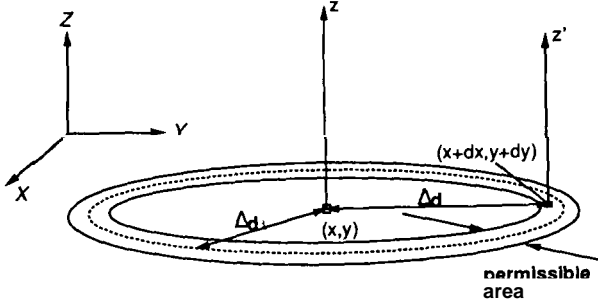


FIG. 3. Accommodating irregular sampling intervals. Because of irregular sampling, we cannot detect a pair of points located a certain distance Δd , away on the xy plane. As a permissible area, we set a circle whose width is 2ϵ around a point (x, y) with z . If the point $(x + dx, y + dy)$ exists in the area, its elevation z' is used to compute A , and B_j .

permissible area including a circle of radius Δd_j (Fig. 3). Suppose there is a data point at $(x + dx, y + dy)$ with elevation z' . If $|\Delta d_j - \Delta d|$ is less than ϵ , then the point lies in the permissible area, and we update the counters A_j , B_j , and C_j as

$$A_j \leftarrow A_j + |z - z'|, \quad B_j \leftarrow B_j + (z - z')^2, \quad C_j \leftarrow C_j + 1.$$

After considering all pairs of data points, we ensure that C_i is larger than a threshold number of pairs. If C_i is small, then we question whether the number of samples was sufficient to compute reliable statistics, and discard this data. Otherwise, we compute the sample standard deviation for Pentland's method by

$$S_{\Delta d_i} = S[|z_{x,y} - z_{x+dx,y+dy}|] = \sqrt{\frac{B_i - (A_i^2/C_i)}{C_i - 1}},$$

and the sample mean for Yokoya's method by

$$E_{\Delta d_i} = E[|z_{x,y} - z_{x+dx,y+dy}|] = A_i/C_i.$$

2. Plot the points in log-log space and identify linear segments.

For Pentland's method, the point coordinates are $(\log \Delta d_i, \log S_{\Delta d_i})$. For Yokoya's method, the point coordinates are $(\log \Delta d_i, \log E_{\Delta d_i})$.

Because most natural patterns exhibit self-similarity only over certain scales, and not over all scales, it is necessary to segment sets of points that are linear. We investigated two approaches to this segmentation problem.

The first approach is polyline fitting using the minimax method, as proposed by Kurozumi [17]. In the field of document image processing, this technique is frequently used to detect line segments. The technique segments the given points into several sets of points which distribute

within narrow rectangles, i.e., nearly along lines. The width of the rectangle must be specified as a threshold. The cardinality of the sets is a natural criterion for determining which should be used to estimate the fractal dimension. However, the cardinality is fairly sensitive to the rectangle width, thus making it difficult to select the proper threshold for this Segmentation technique.

The second approach employs iterative least-square line-fitting [1]. Using this technique, we can construct a set of points that lie within a specified distance of the line. This technique is not sensitive to changes of the threshold. However, the technique selects only the first linear part satisfying the criterion. In the case where several fractal patterns exist, each with a different fractal dimension, multiple linear segments will appear in the log-log plot. Simply selecting the first will preclude consideration of the others. In these experiments, we use one or the other method; a future topic of research is to combine them to identify all of the fractal patterns.

3. Estimate fractal dimension from the slope of linear segments.

When the points lie on a line in the log-log space, we can estimate the fractal dimension of the pattern by the difference between the Euclidean dimension of the pattern and the slope of the line formed by the points.

2.5. Experiments with Synthetic Patterns

We implemented the modified method based on the fractal Brownian function approach, and applied it to sparse synthetic elevation data. We created the data by discarding 95% of the data points, selected randomly from synthetic fractal images (similar to the tops in Figs. 10–12 generated by the Successive Random Addition (SRA) method [28]). Figure 4 plots actual fractal dimension versus the fractal dimension estimated using the modified Yokoya method. The estimated values increases monotonically with the actual fractal dimension, and no saturation occurs. The method tends to overestimate for $D < 2.55$, and to underestimate for $D > 2.55$. The results are similar, although not identical, to those from dense synthetic images (see [1]).

To determine the robustness of the methods against Gaussian noise, we repeated these trials on subsampled synthetic elevations with additive noise distributed $N(0, \sigma_N^2)$, added independently to x , y and $z(\mathbf{d})$. The signal-to-noise ratio (SNR) is computed as $20 \log_{10} \sigma_S / \sigma_N [\text{dB}]$, where the σ_S^2 is the maximum among the variances of x , y and $z(\mathbf{d})$ signals. Figure 4 illustrates the results. Table 1 tabulates the statistics of the fractal dimensions estimated from 100 sets of elevations with various Gaussian random generators. Figure 4 and Table 1 indicate that for SNR of 25 dB or greater, the method computes reasonable estimates

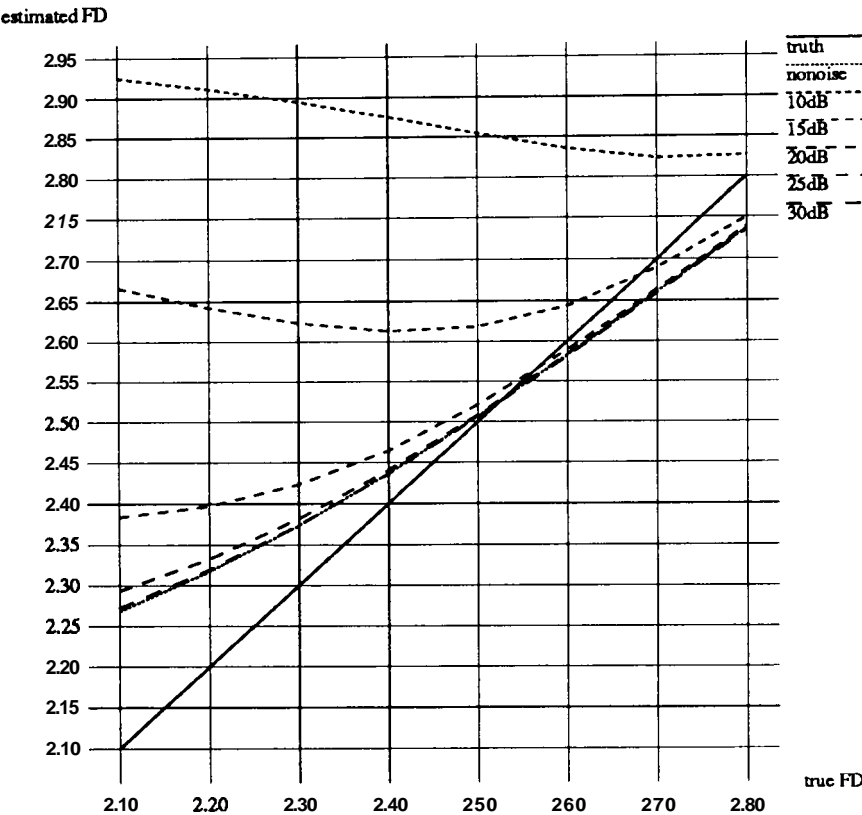


FIG. 4. Errors with Yokoya’s method with irregularly sampled synthesized data. The graph on the left-hand side plots the real fractal dimension against the dimension estimated by the modified Yokoya’s method. The solid line illustrates the ideal relation. The graph on the right-hand side illustrates the effect of Gaussian noise. The dotted and dashed lines represent estimates from data without noise and from data with noise with SNR = 30, 25, 20, 15, and 10 dB.

of the fractal dimension, because significant degradation cannot be seen compared to the estimates from data without noise.

2.6. Experiments with Range Images

In this section, we apply our method to range images acquired with a scanning laser rangefinder manufactured

by Perceptron [18]. The sensor acquires range images with respect to a spherical–polarcoordinate system. Equal sampling intervals in this coordinate system become unequal and irregular when mapped into a Cartesian system. Thus, the data points are not equally spaced when expressed in Cartesian coordinates.

We selected eight patterns from range images acquired

TABLE 1
Estimation Errors of Fractal Dimensions from Irregularly Sampled Elevations with Different Gaussian Noise

True FD	No noise error[%]	SNR = 30 dB			SNR = 25 dB			SNR = 20 dB		
		Mean[%]	Std. dev.	Worst[%]	Mean[%]	Std. Dev.	Worst[%]	Mean[%]	Std. Dev.	Worst[%]
2.1	8.00	8.15	1.30×10^{-3}	8.31	9.16	2.05×10^{-3}	9.35	13.59	3.70×10^{-3}	14.07
2.2	5.18	5.38	1.26×10^{-3}	5.51	5.96	1.94×10^{-3}	6.16	9.02	3.26×10^{-3}	9.38
2.3	3.17	3.20	1.25×10^{-3}	3.33	3.50	1.84×10^{-3}	3.68	5.42	2.90×10^{-3}	5.67
2.4	1.54	1.52	1.25×10^{-3}	1.66	1.67	1.71×10^{-3}	1.83	2.75	2.55×10^{-3}	2.95
2.5	0.28	0.27	1.23×10^{-3}	0.41	0.35	1.58×10^{-3}	0.49	0.88	2.20×10^{-3}	1.06
2.6	0.65	0.68	1.23×10^{-3}	0.79	0.63	1.50×10^{-3}	0.78	0.38	1.89×10^{-3}	0.60
2.7	1.48	1.47	1.19×10^{-3}	1.56	1.42	1.41×10^{-3}	1.56	1.31	1.65×10^{-3}	1.52
2.8	2.29	2.28	1.17×10^{-3}	2.36	2.24	1.34×10^{-3}	2.35	2.17	1.52×10^{-3}	2.37

with the rangefinder. Figures 5–7 illustrate the images, which are presented in order of increasing roughness, as determined subjectively by the authors. We estimated the fractal dimension of the regions indicated by white rectangles.

Before applying the procedures to estimate fractal dimension, we checked whether the data acquired by the rangefinder satisfies the conditions on fractal Brownian functions stated in (2). Figure 8 histograms $z_{x,y} - z_{x+dx,y+dy}$ for Pattern 2, with $\Delta d = 0.4, 0.6$, and 0.8 m. From the figure it is clear that the condition in (2), that $g(x)$ be a cumulative distribution function, is satisfied. We conclude that the patterns are fractal Brownian functions.

A further condition on the distributions, imposed by Yokoya's method, is that they are normal. We conducted χ^2 tests for Gaussianity and observed negative results, i.e., that the probabilities of the data being normally distributed were quite low. This suggests that it is not probable that the points were created by a fractional Brownian motion process (which is a special case of a fractal Brownian function). However, to the extent that the distributions are symmetric, and exhibit a central tendency, there is some justification in proceeding to apply Yokoya's method, despite the negative χ^2 test results.

Figure 9 shows the result of applying Yokoya's method to the range image regions: the points ($\log \Delta d, \log E_{\Delta d}$) segmented by iterative least-square fitting. The points distribute linearly, therefore, we observe self-similarity in all of these natural terrain patterns. On some patterns, plotted points distribute in several sets of linear parts. If we intend to estimate all fractal dimension in such distribution, segmentation by polyline fitting is appropriate. However, we must set a parameter of allowable error for fitting, because the segmentation results are highly sensitive to the parameter.

Table 2 lists the fractal dimensions estimated by Yokoya's method, with both segmentation techniques. Some of the results for segmentation by polyline fitting required careful selection of the amount of allowable error. We also illustrate in parentheses the fitting error normalized by $\log E(\Delta z_{\Delta d})$. All errors are small enough to determine that the patterns are fractal. Moreover, the rows are ordered by roughness, as perceived by the authors. The order of estimated fractal dimension correlate strongly to the intuitive order (the last three patterns—sandy flat floors—are almost identical). These results suggest that the fractal dimension estimated can be utilized as a measure of roughness of natural terrain.

The computational complexity of the method utilized here is $O(N^2)$, where N is the number of pixels, because it is necessary to calculate distances between all pairs of pixels in order to determine which pairs lie in the permissible area. On a Sun4/40 with 24 MB of physical memory, estimating the fractal dimension for Pattern 2 (10,000 pixels)

requires 1.2×10^7 s, and Pattern 5 (19,600 pixels) requires 5.5×10^3 s.

3. FRACTAL RECONSTRUCTION OF NATURAL SURFACES

The surface reconstruction problem can be formulated as follows. Given a scattered set of surface elevation measurements, produce a complete surface representation satisfying three conditions:

- It must take the form of a dense array of inferred measurements with regular spacing.
- It must pass approximately through the original data points.
- It must be smooth where new points are inferred.

The surface reconstruction problem may be called a fitting problem by computer graphics researchers, and an approximation problem by others. It is closely related to the surface interpolation problem, for which the second condition requires the surface to pass exactly through the original data points.

The smoothness constraint in the third condition is inappropriate for natural surfaces, which as a rule exhibit roughness over a wide range of scales [7]. Thus, for the *natural* surface reconstruction problem, the third condition above becomes the following:

- It must be realistically rough where new points are inferred.

This revised condition imposes a requirement that the roughness of the original pattern be known. In turn, this imposes a requirement that the surface reconstruction techniques *adapt* in a nonuniform manner to the roughness of the original pattern.

In this section, we use the estimated fractal dimension to control the roughness of the reconstructed surfaces. Specifically, we estimate the fractal dimension at a coarse scale (given by the spacing of the sensed range data) and use it at a finer scale (between range data samples). This approach relies on the property that as scale changes, the fractal dimension does not.

3.1. Related Research

The surface reconstruction problem has been formulated as an optimization problem, and solutions have been obtained through relaxation methods. For example, Grimson [13] suggested that given a set of scattered depth constraints, the surface that best fits the constraints passes through the known points exactly and minimizes the quadratic variation of the surface. He employed a gradient descent method to find such a surface. Extending this approach to use multiresolution computation, Terzopoulos

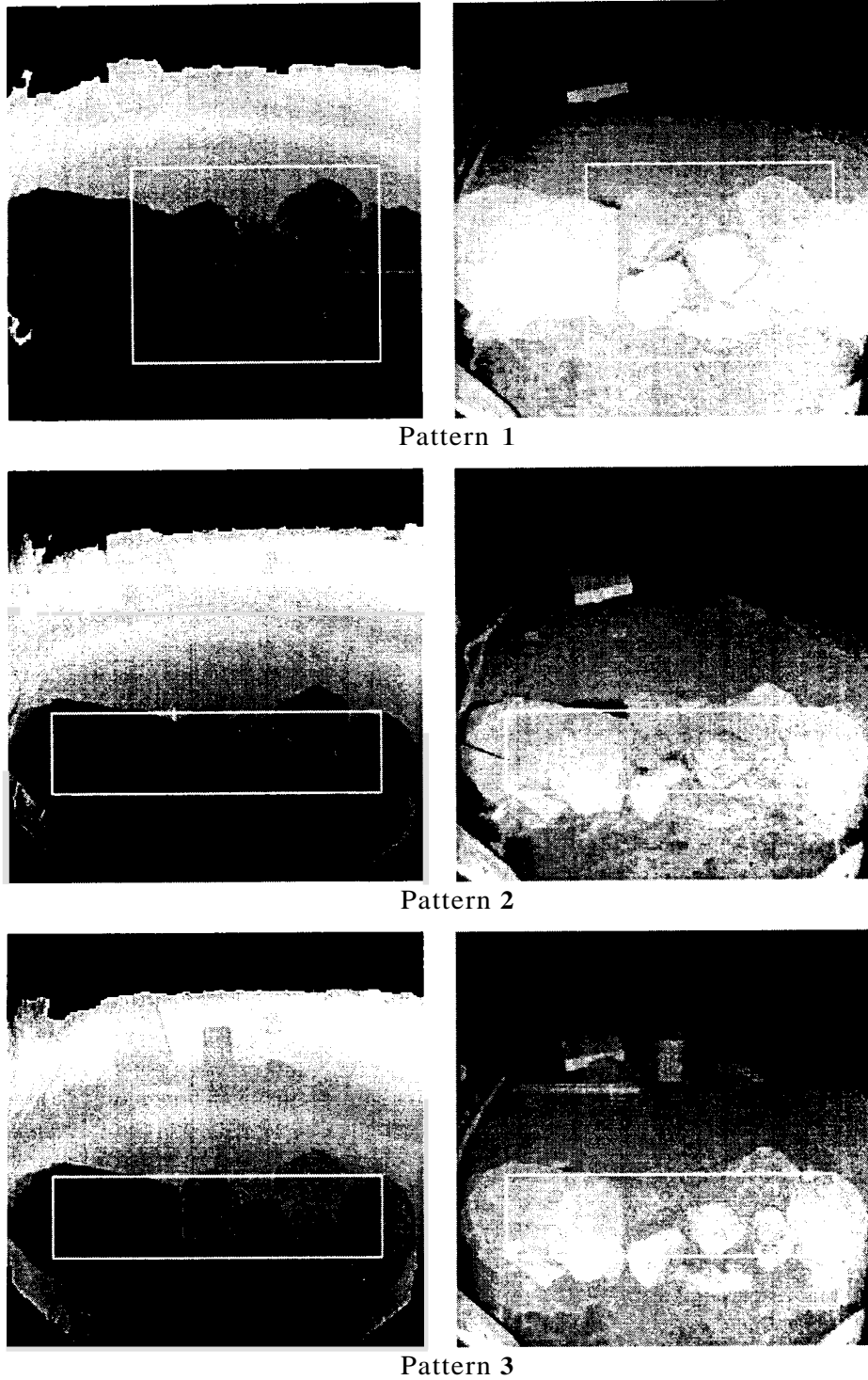
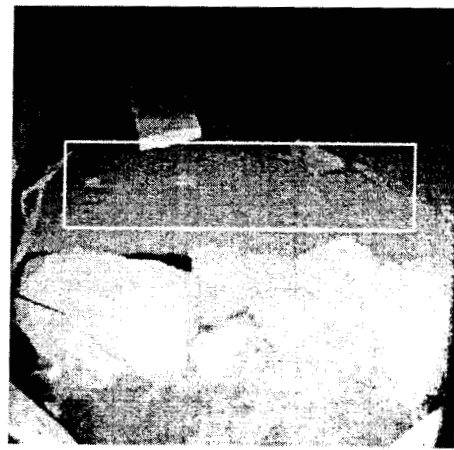
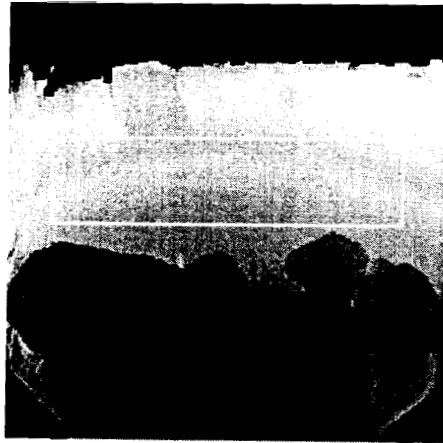
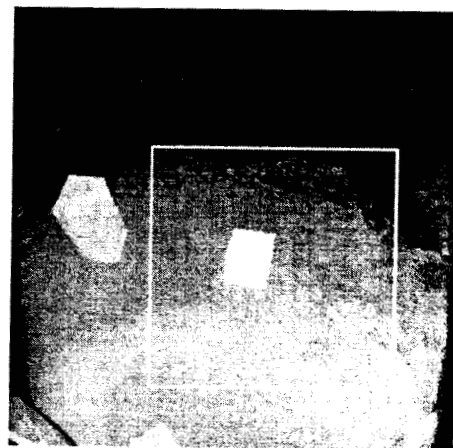
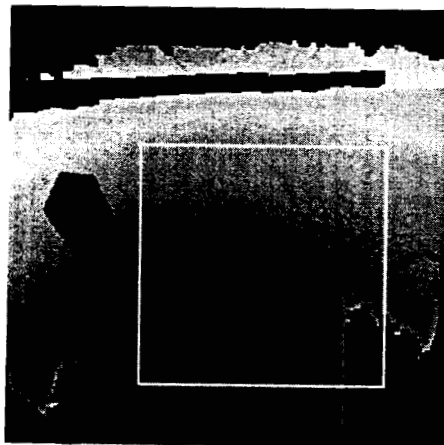


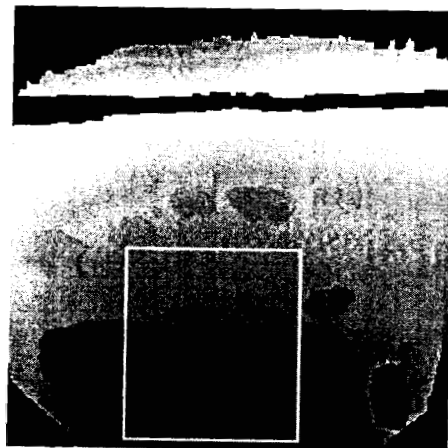
FIG. 5. Rangefinder images (1). The figure illustrates image pairs: processed range (left) and raw reflectance (right). Only the range images are used to estimate fractal dimension.



Pattern 4



Pattern 5



Pattern 6

FIG. 6. Rangefinder images (2).

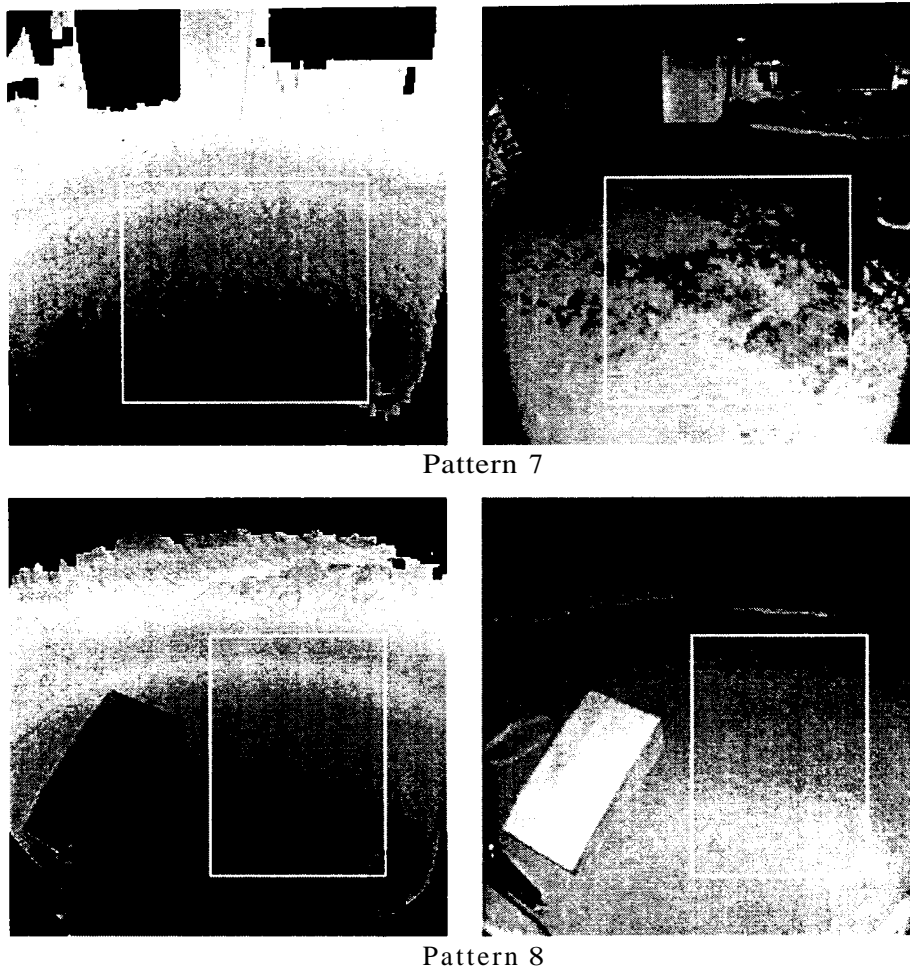


FIG. 7. Rangefinder images (3).

[33] proposed a method minimizing the discrete potential energy functional associated with the surface. In this formulation, known depth and/or orientation constraints contribute as spring potential energy terms. Poggie *et al.* [27] reformulated these approaches in the context of regularization.

Discontinuities in the visible surface have been a central concern in the approaches taken by Marroquin with Markov random fields [24], by Blake and Zisserman with weak continuity constraints [4], and by Terzopoulos with continuation methods [35].

Burt [8] developed a method that relies on locally fitting polynomial surfaces to the data. The method achieves computational efficiency through computation by parts, where the value computed at a given position is based on previously computed values at nearby positions.

Boult [5] developed surface reconstruction methods based on minimization with semireproducing kernel splines, and with quotient reproducing kernel splines. He

compared the time and space complexity of these and other methods for a number of different cases.

Stevenson and Delp [29] presented a two-stage algorithm for reconstructing a surface from sparse constraints. The first stage forms a piecewise planar approximation to the surface, and the second stage performs regularization using a stabilizer based on invariant surface characteristics. By virtue of the selection of stabilizer, the algorithm is approximately invariant to rigid 3D motion of the surface.

The natural surface reconstruction problem has received less attention than the surface reconstruction problem. In the field of approximation, Barnsley [3] introduced iterated function systems with attractors that are graphs of a continuous function f that interpolate a given data set $\{(x_i, y_i)\}$ so that $f(x_i) = y_i$. It appears that these functions are well suited for approximating fractal functions. Barnsley concentrated on existence proofs and moment theory for these functions, and there does not appear to be a firm connection to the issues at hand.

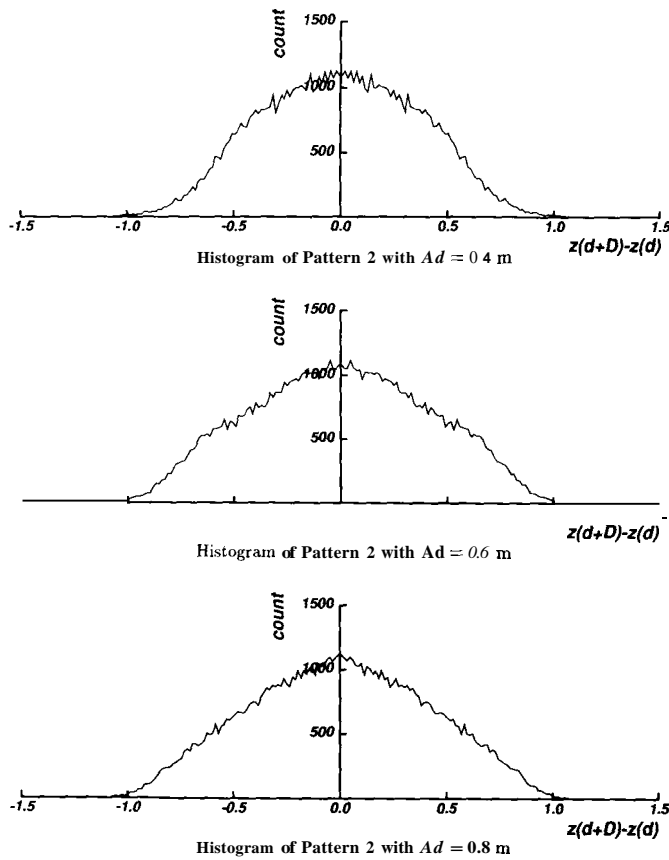


FIG. 8. Empirical distribution functions. These graphs illustrate histograms of $z_{x,y} - z_{x+d,y+d}$ with $Ad = \sqrt{dx^2 + dy^2}$ on Pattern 2.

Yokoya *et al.* [39] present a technique for interpolating shapes described by a fractional Brownian function. The technique follows a random midpoint displacement approach [28]. At each level of recursion, the midpoint is determined as a Gaussian random variable whose expected value is the mean of its four nearest neighbors. Next, the technique displaces this midpoint by an amount that depends on the fractal dimension and the standard deviation of the fractional Brownian function. Thus, their technique is both stochastic and adaptive. However, there are key limitations:

1. The technique requires an equal spacing between samples of the original pattern.
2. The technique cannot generate stationary random fractals. This is a result of a compromise between computational expense and generality.
3. The technique, like a midpoint displacement method,¹ cannot generate stationary random fractal increments [21].

¹ Some modified techniques [28, 30] have been proposed to solve the nonstationary increment problem.

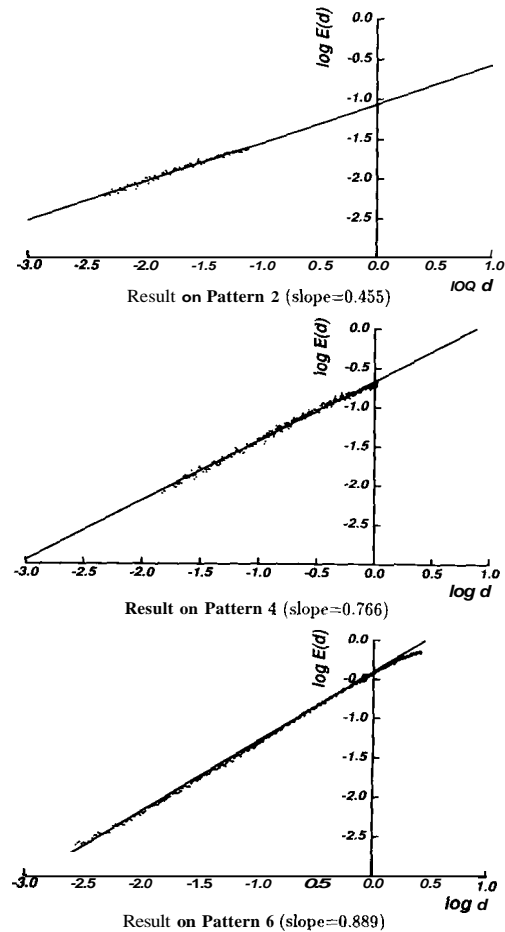


FIG. 9. Results with Yokoya's method on rangefinder images. These graphs illustrate the segmented points and the lines fitted to them. The label $(\log d, \log E(d))$ corresponds to $(\log \Delta d, \log E_{\Delta d})$ in the text.

Szeliski [32] showed that regularization based on the thin-plate model and weak-membrane model generates fractal surfaces whose fractal dimensions are 2 and 3.

TABLE 2
Fractal Dimensions Estimated with Different Linear Segmentations

Pattern	D (error) LSF	D (error) Polyline
1	2.691 (0.012)	2.661 (0.025)
2	2.545 (0.021)	2.512 (0.016)
3	2.498 (0.016)	2.486 (0.014)
4	2.234 (0.024)	2.239 (0.025)
5	2.210 (0.009)	2.196 (0.010)
6	2.111 (0.018)	2.118 (0.021)
7	2.090 (0.009)	2.102 (0.014)
8	2.038 (0.018)	2.010 (0.022)

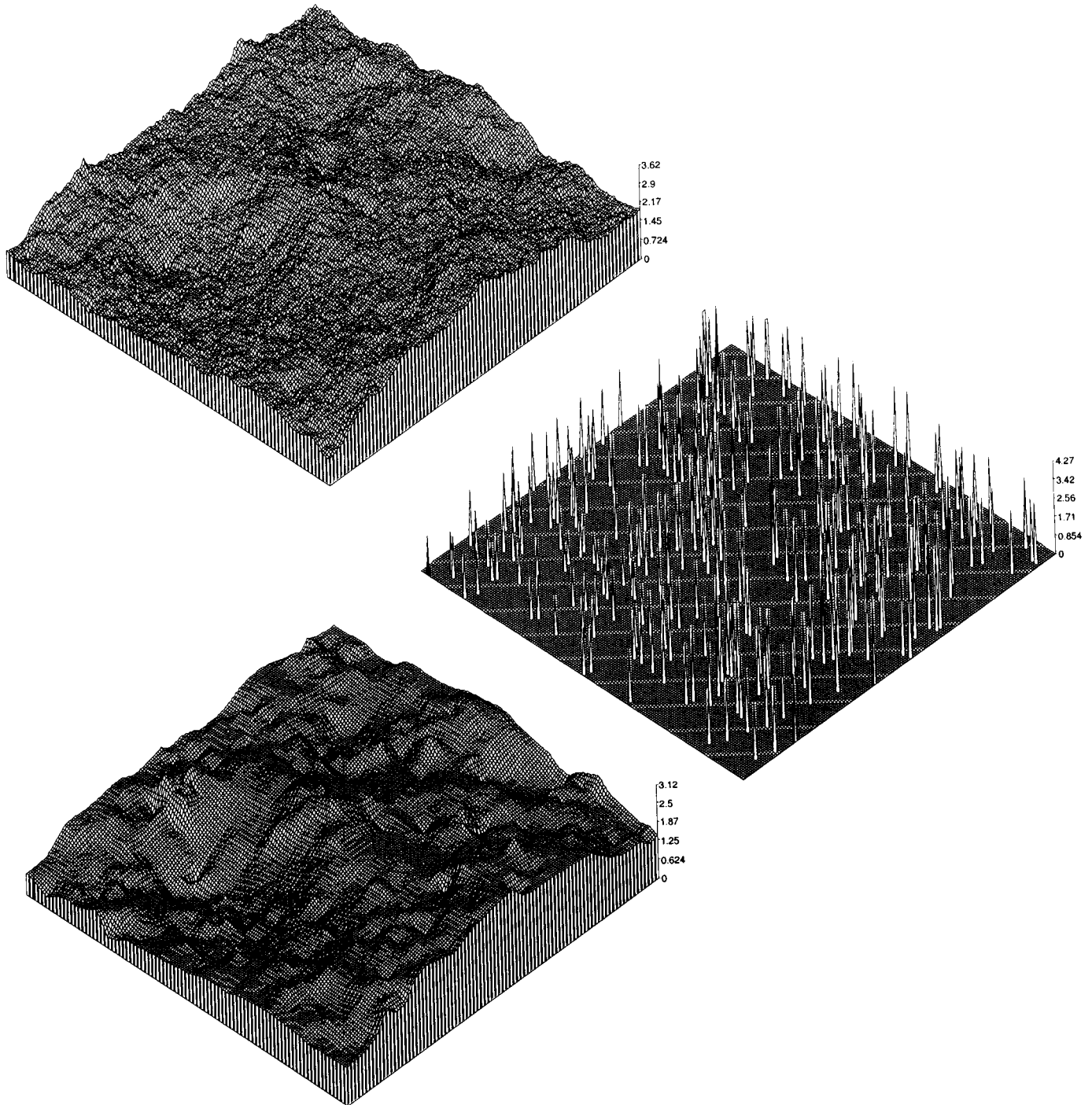


FIG. 10. Reconstruction of synthetic surface ($D = 2.3$) using Szeliski's method. (top to bottom) Synthetic original, subsampled, and reconstructed surfaces.

respectively. He then developed a probabilistic method for visual surface reconstruction using Maximum A Posteriori (MAP) estimation based on the fractal prior (see Section 3.2). The method generates surfaces whose fractal dimension lies between 2 and 3. Szeliski's approach

provides the central inspiration for this work. Our contribution is to extend his approach, amending a number of technical details concerning the temperature parameter, and applying the extended approach to nonsynthetic range data from natural terrain.

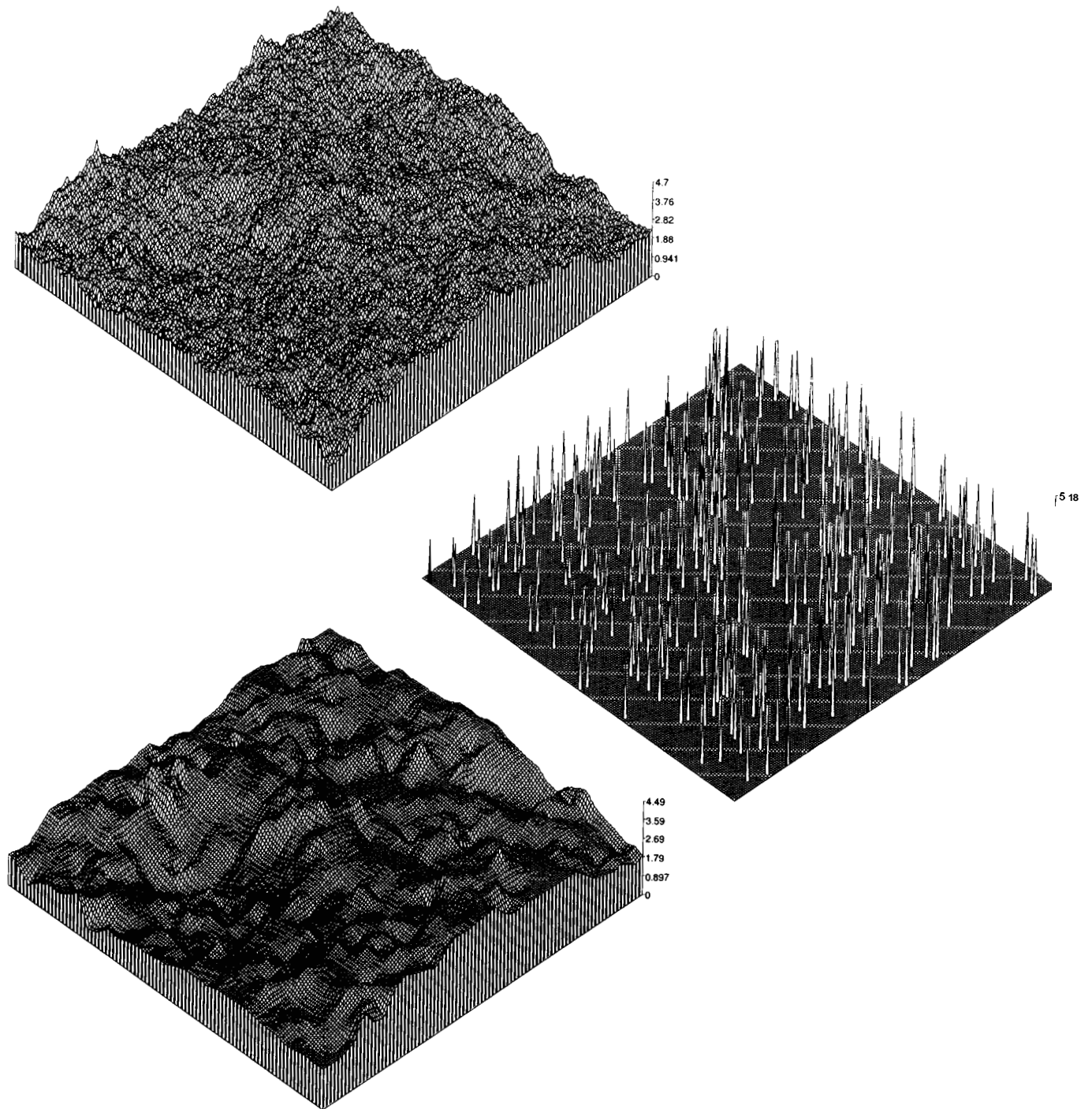


FIG. 11. Reconstruction of synthetic surface ($D = 2.5$) using Szeliski's method. (top to bottom) Synthetic original, subsampled, and reconstructed surfaces.

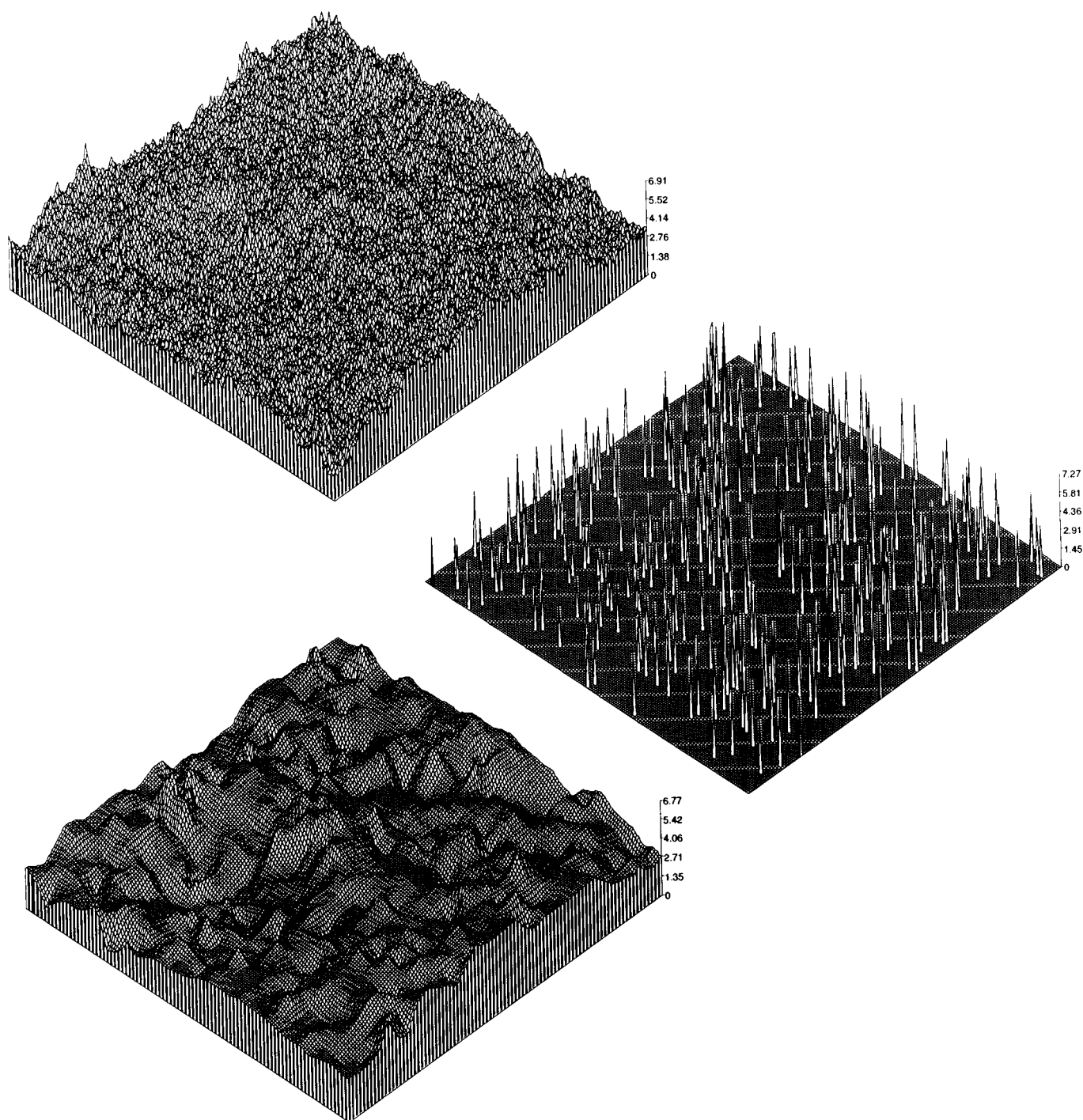


FIG. 12. Reconstruction of synthetic surface ($D = 2.7$) using Szeliski's method. (top to bottom) Synthetic original, subsampled, and reconstructed surfaces.

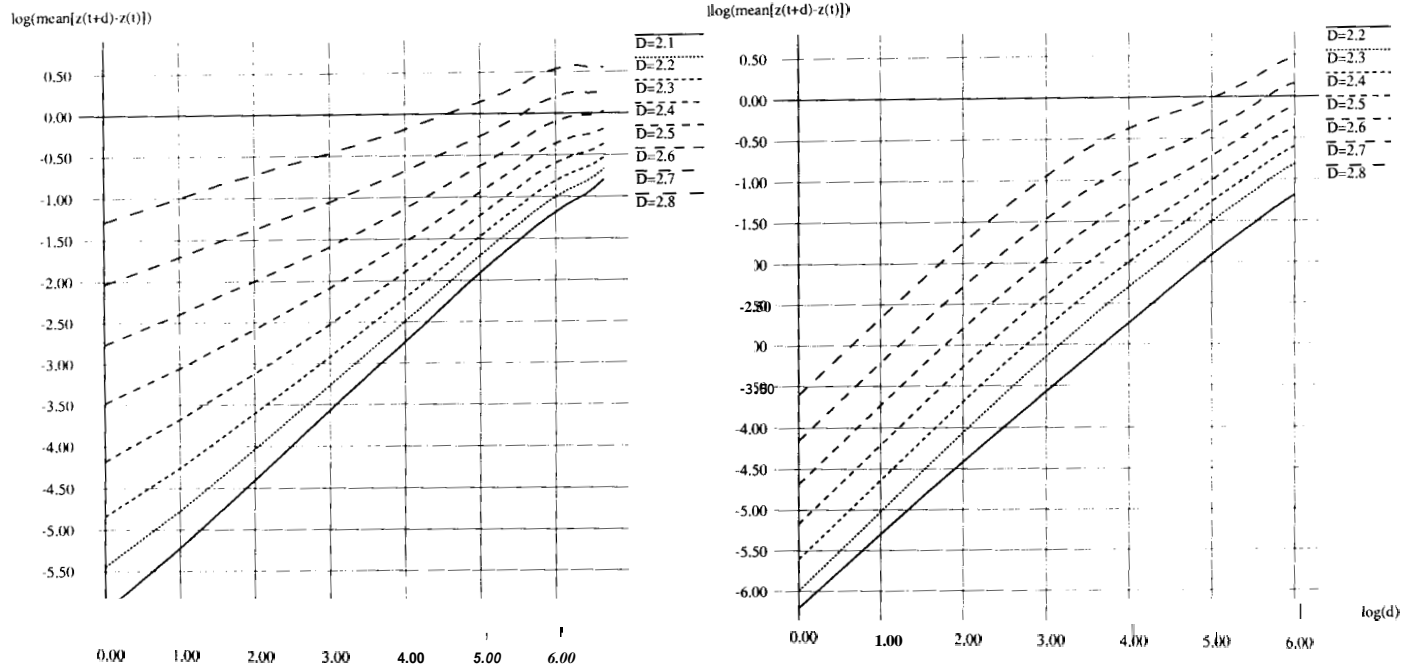


FIG. 13. Scaling behavior of original (left) and reconstructed (right) surfaces.

3.2. Regularization Using Fractal Priors

Szeliski [31, 32] developed a Bayesian framework for interpolating sparse elevation data that uses MAP estimation, and fractal prior distributions. In his formalization, the maximization of a posteriori probability is similar to the minimization of energy performed by regularization. For energy minimization, he employs a multigrid representation of the data called the *relative multiresolution decomposition*. For surface reconstruction, he minimizes the energy in each layer l (from the coarsest layer to the finest layer)

$$E^l(\mathbf{u}_l) = E_d(\mathbf{I}\mathbf{u}_l, \mathbf{d}) + E_p^l(\mathbf{u}_l)/T_p. \quad (6)$$

The term E_d in (6) is the data compatibility energy

$$E_d = \frac{11}{2} \sum_{(i,j)} c_{i,j} (u_{i,j} - d_{i,j}),$$

where $u_{i,j}$ is an absolute elevation computed using an interpolation matrix \mathbf{I} that computes absolute elevations from the relative elevations in the multiresolution decomposition, and $d_{i,j}$ is a given elevation value. The term $c_{i,j}$ represents the confidence in $d_{i,j}$ typically given by the inverse of the measurement error.

The term $E_p(u)$ in (6) is the prior constraint energy, formulated as a blend of the thin-plate and weak-membrane models (called "splines under tension" by Terzopoulos [34])

$$E_p^l(u_l) = \frac{1}{2} \iint [w_1^l(u_{lx}^2 + u_{ly}^2) + w_2^l(u_{lxx}^2 + 2u_{lxy}^2 + u_{lyy}^2)] dx dy,$$

where the weights are

$$w_1^0 = |2\pi f_0| w_2^0, \quad (7)$$

$$w_m^{l+1} = 2^{2(m+D-4)} w_m^l, \quad (8)$$

and D is the fractal dimension.

The parameter T_p in (6) is similar to the temperature for the Gibbs sampler developed by Geman and Geman [12]. At higher temperatures, the local conditional probability distributions become more uniform.

TABLE 3
Temperatures Determined
Empirically for Synthetic Data

D	T_p	$ D - \hat{D} $
2.2	9.5×10^{-6}	7.0×10^{-3}
2.3	3.0×10^{-5}	2.1×10^{-2}
2.4	8.9×10^{-5}	3.0×10^{-3}
2.5	3.0×10^{-4}	1.9×10^{-2}
2.6	7.5×10^{-4}	8.0×10^{-3}
2.7	3.0×10^{-3}	1.0×10^{-3}
2.8	9.5×10^{-3}	5.1×10^{-2}

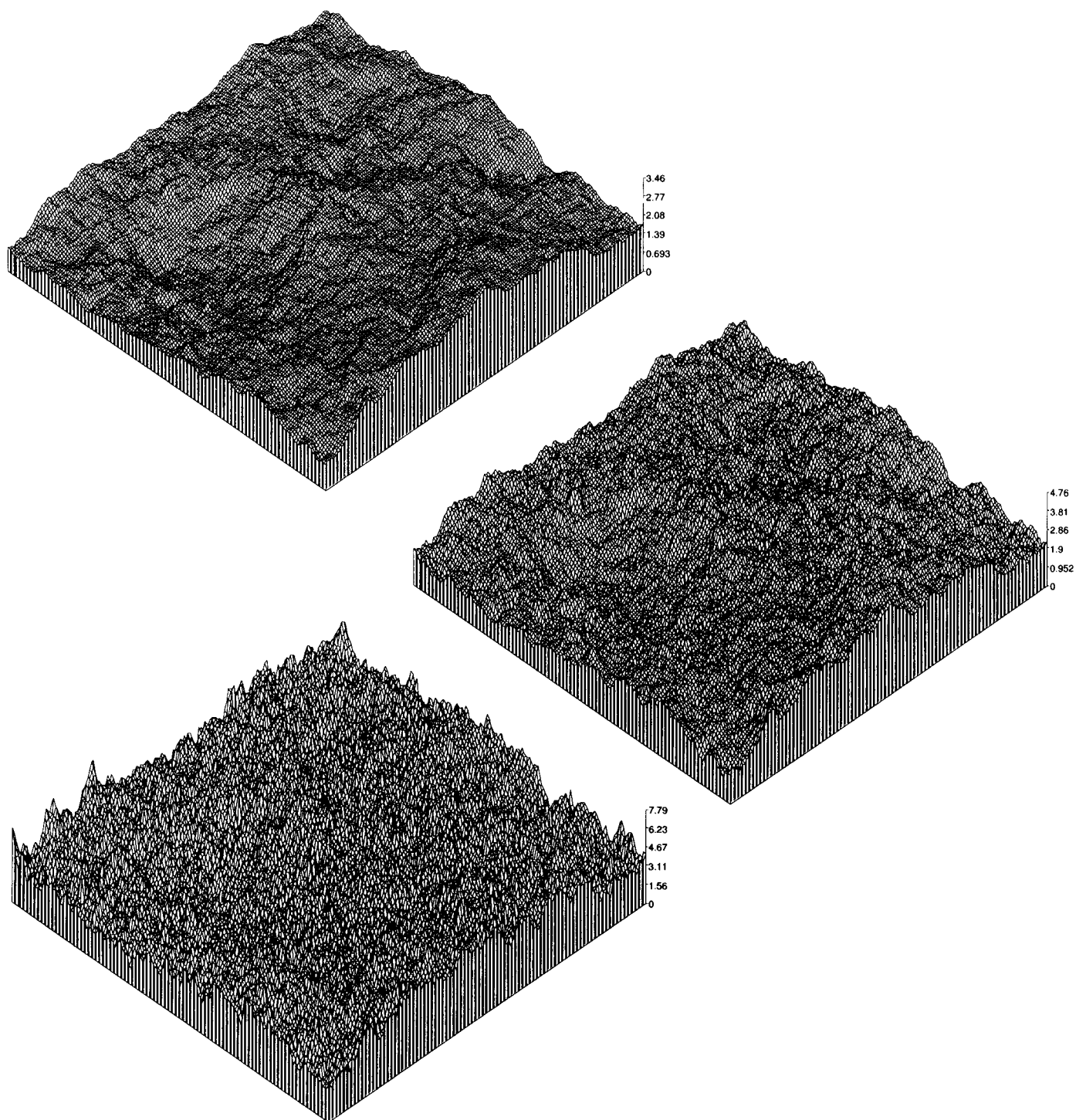


FIG. 14. Surfaces reconstructed from synthetic data using nonzero temperatures. From top to bottom, the fractal dimensions are set to 2.3, 2.5, and 2.7. The original synthesized and subsampled elevations are the same as for Figs. 10–12.

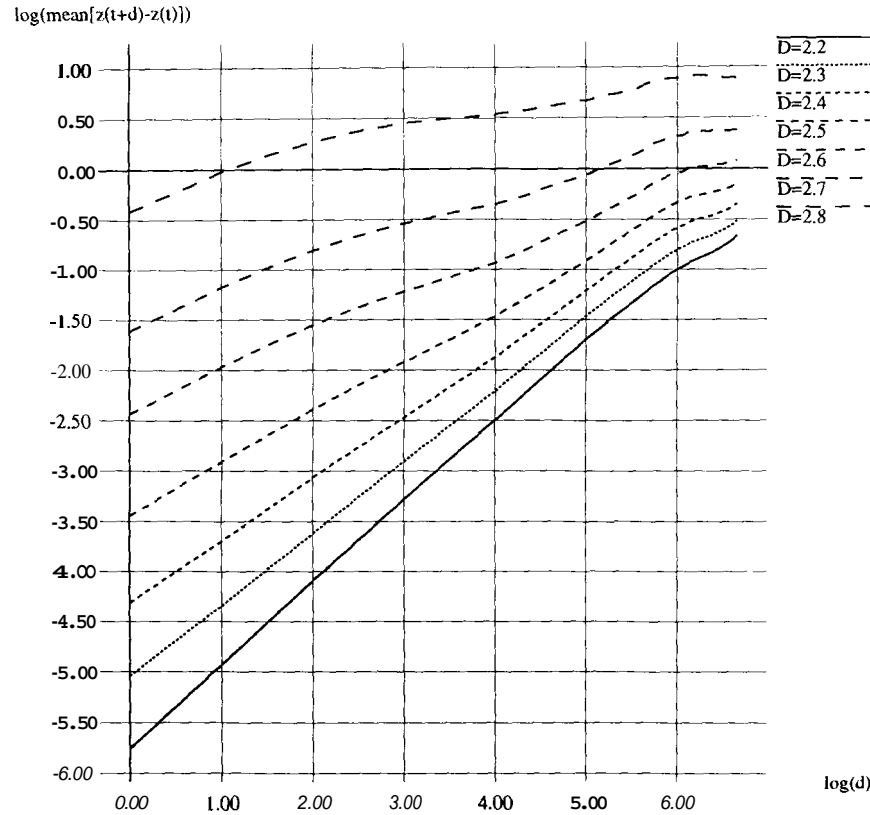


FIG. 15. Scaling behavior of reconstructions using nonzero temperatures.

Using (7), Szeliski found empirically that minimizing the energy of only the finest layer, the prior model behaves as a fractal whose dimension is D in the vicinity of frequency f_0 . Equation (8) changes the frequency, thus varying the fractal dimension of different resolutions in the multiresolution decomposition.

Szeliski applied Gauss–Seidel relaxation for energy minimization. The energy can be rewritten in the quadratic form

$$E(u) = \frac{1}{2} \mathbf{u}^T \mathbf{A} \mathbf{u} - \mathbf{u}^T \mathbf{b} + c \quad (9)$$

$$= \frac{1}{2} (\mathbf{u} - \mathbf{u}^*)^T \mathbf{A} (\mathbf{u} - \mathbf{u}^*) + k, \quad (10)$$

with $\mathbf{A} = \mathbf{A}_p/T_p + \mathbf{A}_d$, $\mathbf{b} = \mathbf{A}_d \mathbf{d}$, and the optimal elevations that minimize the energy $\mathbf{u}^* = \mathbf{A}^{-1} \mathbf{b}$. Because the energy term is quadratic, the relaxation method reaches the minimum energy, and the optimal elevations are computed with $T_p = 0$.

The probability distribution corresponding to the energy function is

$$p(u_i | \mathbf{u}) \propto \exp \left(-\frac{a_{ii}(u_i - u_i^+)^2}{2T_p} \right),$$

which is a Gaussian with mean u^+ and variance T_p/a_{ii} (also called a Gibbs or Boltzmann distribution). Thus, setting T_p to a nonzero value changes the variance (“noise”) of the reconstructed surface.

3.3. Effect of Temperature on Surface Reconstruction

The temperature parameter T_p controls the diffusion of the local energy distribution [32]. Do the fractal characteristics of the reconstructed surface depend on T_p ?

TABLE 4
Temperatures Determined by New
Formalization for Synthetic Data

D	D^*	T_{p0}	$(D^* - \hat{D})$
2.2	2.236	4.4×10^{-6}	6.0×10^{-2}
2.3	2.308	1.5×10^{-5}	4.4×10^{-2}
2.4	2.390	4.5×10^{-5}	2.6×10^{-2}
2.5	2.476	1.4×10^{-4}	1.8×10^{-2}
2.6	2.561	4.1×10^{-4}	1.7×10^{-2}
2.7	2.643	1.3×10^{-3}	3.5×10^{-2}
2.8	2.716	3.8×10^{-3}	5.6×10^{-2}

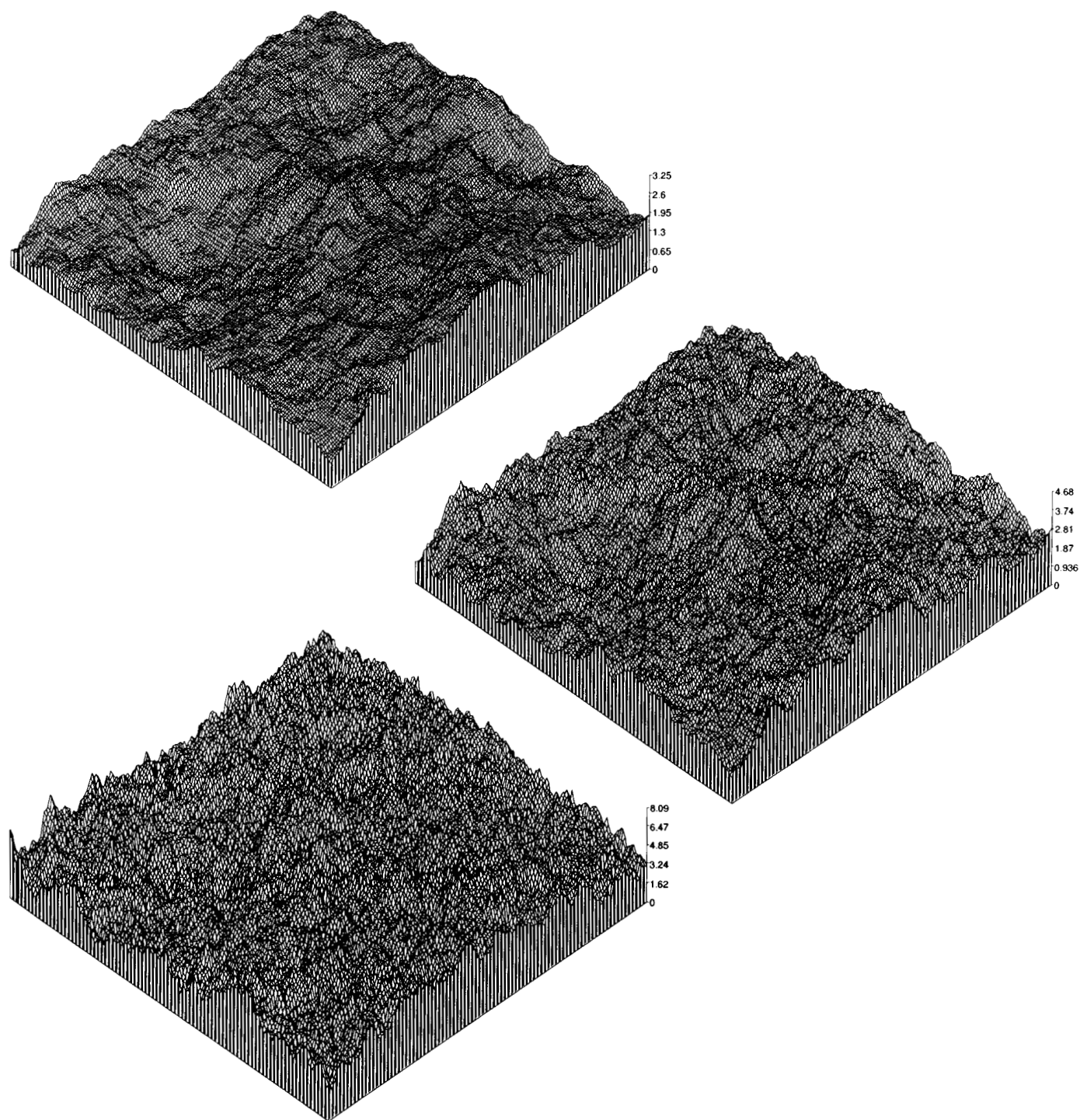


FIG. 16. Surfaces reconstructed using temperatures computed by new formalization. From top to bottom, the fractal dimensions are set to 2.3, 2.5, and 2.7. The original synthesized and subsampled elevations are the same as for Figs. 10–12.

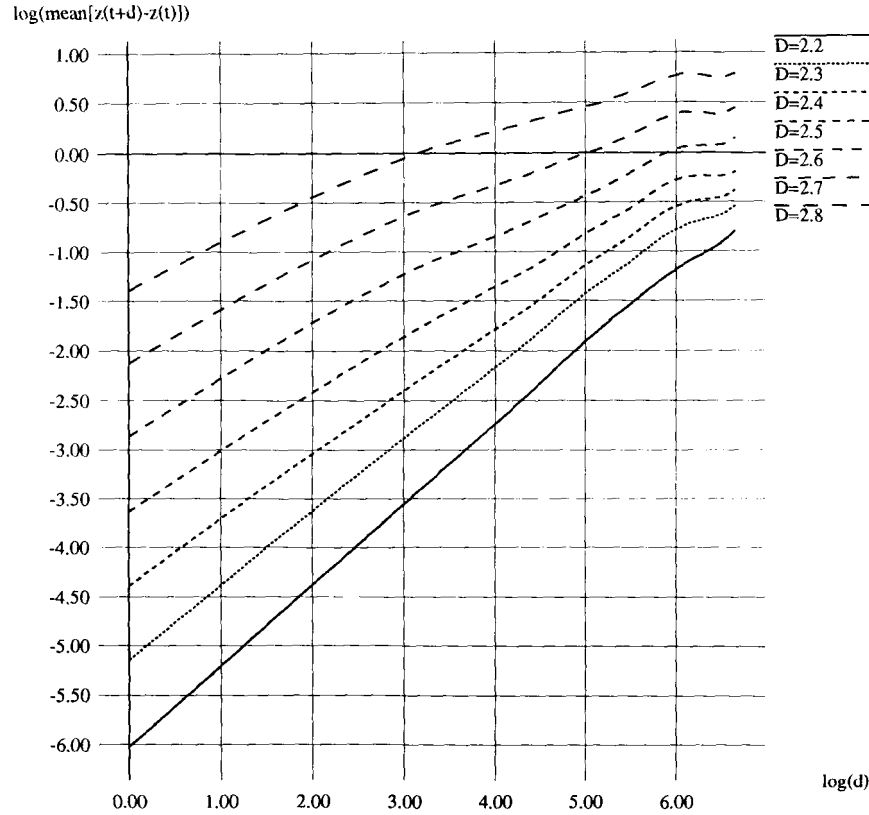


FIG. 17. Scaling behavior of surfaces reconstructed using new temperatures.

To answer this question, we synthesized eight elevation maps with fractal dimensions varying from 2.1 to 2.8. We subsampled these elevation maps, set T_p to zero, and then reconstructed the subsamples. Figures 10–12 depict the reconstructed surfaces for fractal dimensions 2.3, 2.5, and 2.7. In each case, the reconstructed result is too smooth, as compared to the original synthetic patterns.

Figure 13 plots estimates, using Yokoya's method, of the fractal dimension of the eight reconstructed surfaces. More precisely, the figure illustrates the scaling characteristics of the underlying data: the abscissa represents logarithmic scale (e.g., over what size neighborhood is the estimate computed), and the ordinate represents logarithmic spatial variation (e.g., the amount of variation in surface elevation). If the underlying data possesses fractal characteristics, then the curve in the log–log plot will be linear over a wide range of scales, and the slope of the line will vary inversely with the fractal dimension (the greater the slope, the smaller the fractal dimension).

Results for the eight original synthetic data sets appear on the left-hand side of Fig. 13. The curves exhibit linear behavior over most scales; the departure from linearity at larger scales is an artifact of the technique for estimating the fractal dimension.

Results for the reconstructions appear on the right-hand side of Fig. 13. To zeroth order, the curves are parallel, implying (incorrectly) that the surfaces have the same fractal dimension. To first order, analysis reveals that the slope in each of the plots is too steep at higher frequencies (smaller scales); i.e., the fractal dimension of the reconstructed surfaces is too low. This is also apparent, qualitatively, in the reconstructions shown in Figs. 10–12. These results demonstrate that surface reconstruction using a temperature of zero produces overly smooth surfaces, at least at higher frequencies. Thus, the answer is affirmative to the question of the dependence of fractal characteristics on T_p .

Since setting T_p to zero produces unsatisfactory reconstructions, what is the proper T_p for a given fractal dimen-

TABLE 5
Temperatures Determined by New
Formalization for Range Data

D^*	T_{p0}	$ D^* - \hat{D} $
2.12	1.0×10^{-7}	1.0×10^{-1}
2.23	1.8×10^{-7}	4.5×10^{-2}
2.51	1.0×10^{-4}	1.6×10^{-2}

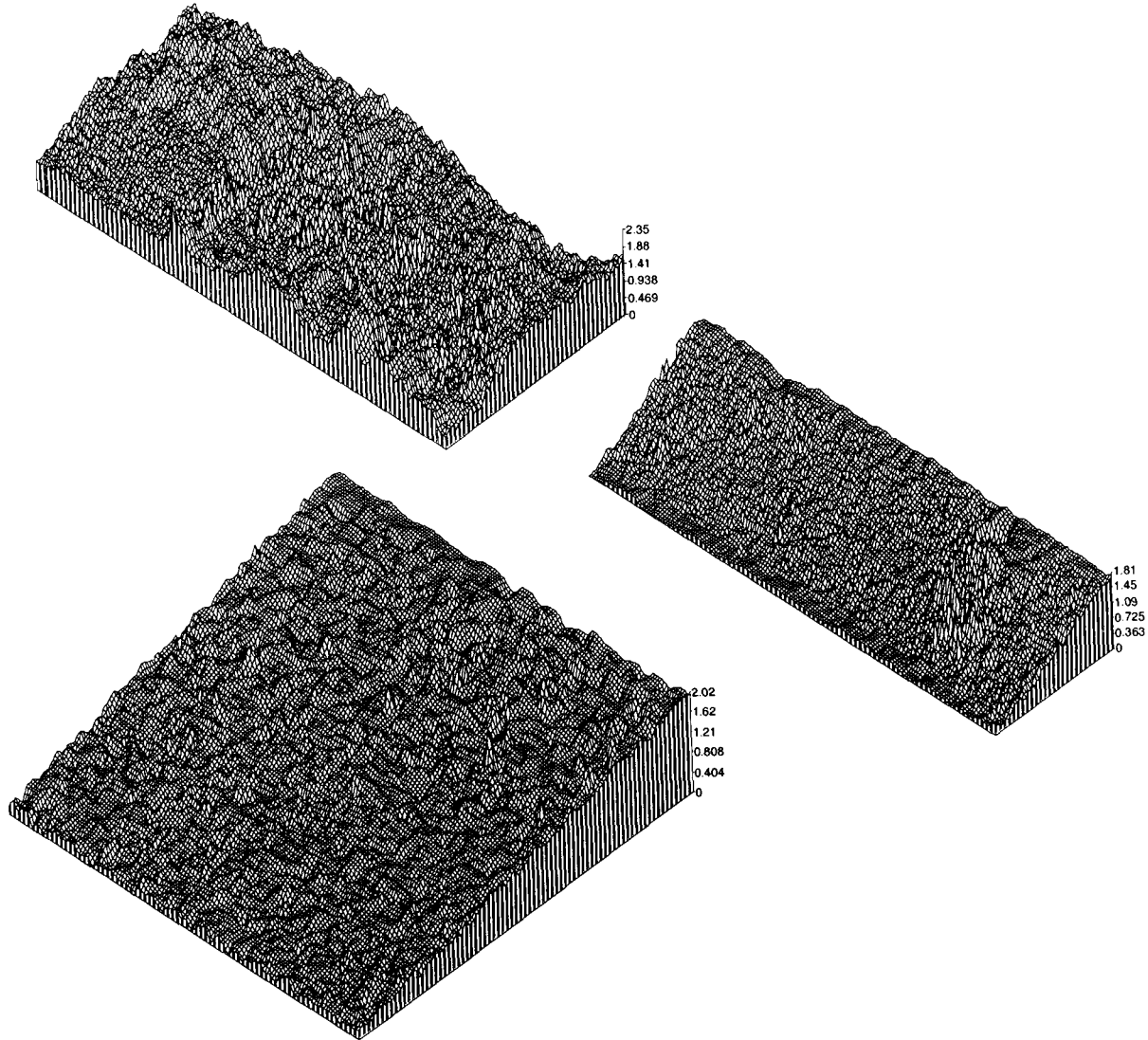


FIG. 18. Surfaces reconstructed from range data. The range data was acquired for rocky terrain (top) and two different sandy terrains (middle and bottom).

sion D ? To answer this question empirically, let $\text{Syn}()$ synthesize a dense fractal pattern of fractal dimension D , $\text{Sub}()$ subsample a pattern, $\text{Rec}()$ reconstruct a pattern using regularization with temperature T_p , and $\text{Est}()$ estimate the fractal dimension of a pattern (again, using Yokoya's method). Let D be given by

$$\text{Est}(\text{Rec}(\text{Sub}(\text{Syn}(D)), T_p)) = \hat{D}. \quad (11)$$

The proper temperature T_p for D is that which minimizes the difference between D and \hat{D} . When searching for the minimum difference, we use the estimated fractal dimension $D^* = \text{Est}(\text{Syn}(D))$ instead of D , because the estimated

fractal dimension is apt to be smaller than the real fractal dimension, especially for $D > 2.5$.

Table 3 records seven empirically determined temperatures, and the differences between the fractal dimension of the original patterns and of the reconstructed results. All the differences are small, lending credence to the conclusion that setting T_p appropriately permits the method to preserve the roughness of the original patterns, even on reconstructed surfaces,

Figure 14 shows surface reconstructions using three of the empirically determined temperatures. The reconstructed surfaces are reasonably rough compared to the original synthetic patterns.

Figure 15 plots the estimated fractal dimension of the

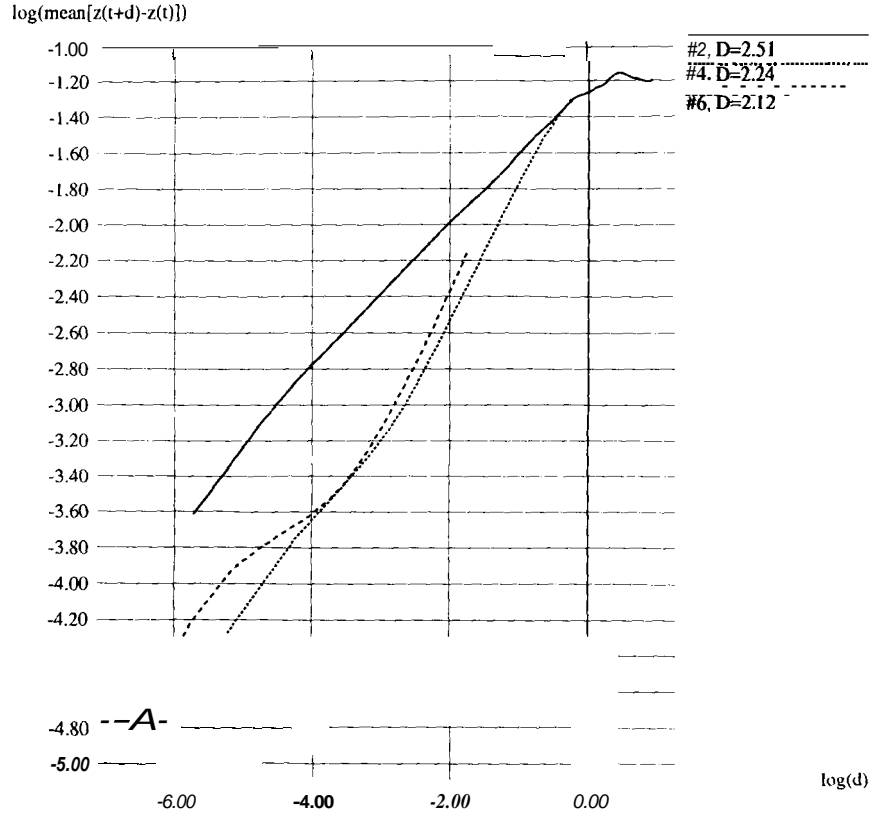


FIG. 19. Scaling behavior of reconstructions from range data with new temperatures

reconstructed results. The curves display fairly linear behavior over most scales, and unlike the right-hand side of Fig. 13, they no longer appear parallel or exhibit steep slopes at higher frequencies.

3.4. Temperature as a Function of Fractal Dimension

The results from the previous section demonstrate control over the fractal characteristics of the reconstructed surface by setting appropriate nonzero temperatures. However, the temperatures do not appear to have any meaning regarding fractal dimension; the temperatures simply control the amount of local diffusion [32]. In this section, we formalize the temperatures as a function of fractal dimension using an analogy to the **SRA** method.

The **SRA** method synthesizes fractional Brownian motion. It adds normally distributed random values to elevations in the multigrid representation. The variances are controlled according to the resolution of each layer l by

$$\sigma^2 = \frac{\sigma_0^2(1 - 2^{4-2D})}{2^{(6-2D)l}},$$

where D is the fractal dimension of the pattern to be synthesized.

Szeliski's method adds a normally distributed random value to the elevations of each layer in the multigrid representation by setting a nonzero temperature T_{pl} . The temperature is proportional to the variance of the Gaussian, and controls the amount of diffusion in the high-frequency domain. His method uses the same temperature (same variance) for all layers.

In order to synthesize patterns that preserve fractalness at higher frequencies, we set the temperature T_{pl} at each layer l by analogy with the **SRA** method

$$T_{p0}(D) = k\sigma_0^2(1 - 2^{4-2D}), \quad (12)$$

$$T_{pl}(D) = T_{p,l-1}(D)2^{6-2D}, \quad (13)$$

where $T_{p0}(D)$ is the temperature for the finest-resolution layer, and σ_0 is the standard deviation of elevation values sampled at the finest resolution.

The two unknowns are σ_0 and k . Pentland's method for fractal dimension estimation [26] directly computes the parameter σ_0 . To compute k , it suffices to know one temperature $T_{p0}(D)$, and then to follow the iterative method taken in the previous section to determine the proper temperatures.

To test this formalization of temperature as a function

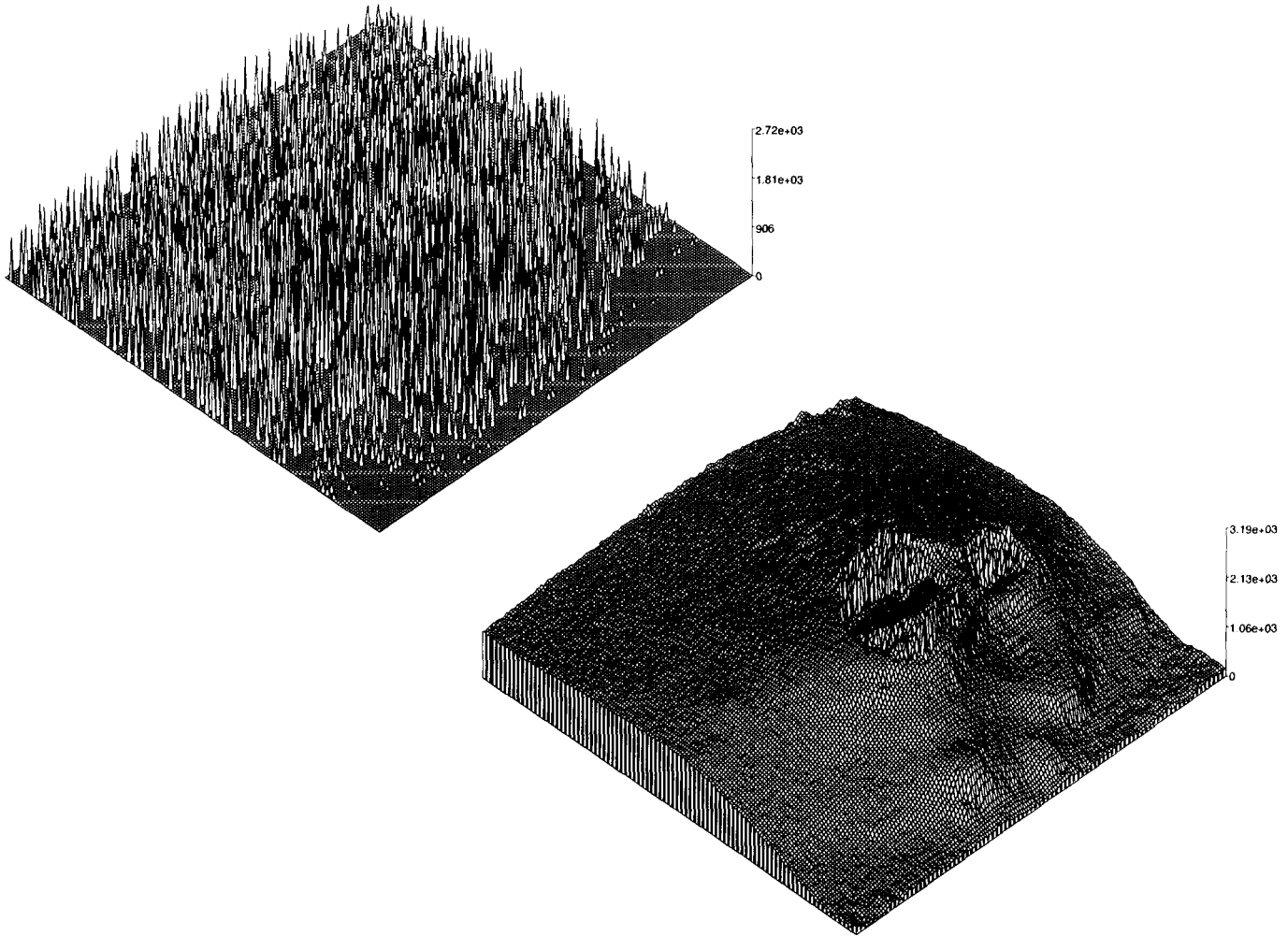


FIG. 20. Surface reconstructed from digital terrain data for Mt. Erebus. Original elevation data (**top**) and reconstructed surface when the fractal dimension is set to 2.65 (**bottom**).

of fractal dimension, we applied it to three different types of data: synthetic data, range data from a scanning laser rangefinder, and digital terrain map data.

For synthetic data, we first determined $T_{p0}(D)$ for $D = 2.4$. From this known temperature, it follows that $k = 4.7 \times 10^{-7}$. Using this value of k , Eqs. (12) and (13) compute temperatures for different D . Table 4 records the computed temperatures, as well as the difference between the fractal dimension $D^* = \text{Est}(\text{Syn}(D))$ and the fractal dimension D given by (11). The differences between D^* and \hat{D} are negligible.

Figure 16 illustrates the surfaces reconstructed using these new temperatures. The surfaces appear appropriately rough and highly realistic. Figure 17 plots the estimated fractal dimension of the reconstructed surfaces. It shows that the reconstructed surfaces maintain linearity over a wide range of scales.

We acquired range data from laser rangefinder images

of a test area with sand on the ground, and some meter-scale rocks. We selected a relatively smooth area of the terrain consisting mainly of sand. We computed the proper temperature for this pattern and calculated k as 4.0×10^{-2} . Table 5 shows the temperatures computed using this value of k . The differences between D^* and \hat{D} are comparable to those observed for synthetic data (Table 4).

Figure 18 shows three reconstructed surfaces. The top surface is reconstructed from data corresponding to a rougher area of the terrain consisting mainly of rocks, and the other surfaces are reconstructed from data corresponding to smoother areas consisting mainly of sand. Using the same parameters (k , σ_0 , T_{p0}), the method adapts to the roughness of the original surface, reconstructing the rocky

² The parameter k is constant for patterns of any fractal dimension, so long as they are generated by the same process. For this new data, a different generating process acts. Therefore, we must recompute k .

area rather roughly, and reconstructing the sandy area rather smoothly.

Figure 19 plots the scaling behavior of the reconstructed elevation maps. These are not as linear as for the synthetic data. However, they do exhibit enough of a linear tendency to demonstrate scale-invariance.

We acquired digital terrain data from an aerial cartography database of Mount Erebus, an active volcano in Antarctica. We estimated the fractal dimension D^* to be approximately 2.3, with $\sigma_0 \approx 68.0$. We used the value of k determined above for the range data, and reconstructed the sparse data. Figure 20 shows that the method produces results that are dense and fairly realistic, including even the shape of craters.

Our approach requires large amounts of computation. Reconstruction of a 256×256 elevation map typically consumes around 2 h on a Sun4/75 with 24 MB physical memory. The surface reconstruction approach has been implemented on a massively parallel machine, reducing substantially the computation time (a speedup of 100 for a 64K MasPar) [40].

4. DISCUSSION

In this paper, we addressed two issues in fractal modeling of natural terrain: estimation of fractal dimension, and fractal surface reconstruction.

With respect to the first issue, we investigated the fractal Brownian function approach to the problem of estimating fractal dimension. We extended published algorithms to accommodate irregularly sampled data supplied by a scanning laser rangefinder, and applied the extended methods to noisy range imagery of natural terrain (sand and rocks). The resulting estimates of fractal dimension correlated closely to the human perception of the roughness of the terrain. We conclude that it is reasonable and practical to model natural terrain as a fractal pattern, and that the fractal dimension is a reasonable measure of roughness of terrain.

Problems remaining to be addressed include determining the region in which to conduct fractal analysis, identifying which linear parts of the log-log curves are most significant, and segmenting multifractal patterns. We may need further simulations using different noise models (e.g., non-Gaussian additive noise, quantization, and truncation) in order to study the sensitivity of methods to estimate fractal dimension, and to determine how appropriate the estimation is.

With respect to the second issue, we described an approach to fractal surface reconstruction that produces dense elevation maps from sparse inputs. The reconstruction stochastically performs energy minimization using regularization, in which the prior knowledge terms include roughness constraints, and in which the temperature term

depends on the fractal dimension. We demonstrated the method using sparse elevation data from rugged, natural terrain, and showed that it adaptively reconstructs surfaces depending on the roughness of the original data. The reconstructed elevations are realistic and natural.

As future work, we consider two topics. First, our surface reconstruction approach does not take discontinuities into account. Natural terrain contains many discontinuities, such as step edges around stones. Our method does not produce realistic results reconstructing sparse depth data with discontinuities. Many researchers have considered this problem and have derived methods that we expect will fit well with our approach.

In nature and more frequently in artificial scenes, many patterns are not truly self-similar, but are anisotropic and/or the fractal dimension changes with scale or changes spatially. Several methods for handling such patterns have been reported in the literature. Bruton and Bartley [6] have shown a method to generate fractal images with spatially-variant characteristics. Kaplan and Kuo [14] proposed a method to synthesize scale-variant fractal textures using the extended self-similar (ESS) model. Our approach cannot be applied to such patterns directly. However, the MAP-based method can interpolate the surfaces with spatially-variant roughness [32]. Further, our approach can change the roughness at a specific scale by controlling the temperature at each resolution.

Another future work should identify the sensitivity of our fractal interpolation method, determining the change in fractal dimension caused by small variations in the temperature settings. This work will be important for applications requiring small surface roughness tolerances.

In conclusion, fractal dimension is a powerful descriptor of natural terrain, a descriptor related to the ambiguous property of roughness. We expect that our contributions—analysis and surface reconstruction using fractal dimension—will advance fractal modeling of natural terrain beyond mathematical curiosity, and closer to practical applications.

ACKNOWLEDGMENT

The authors thank Dr. Richard Szeliski and Dr. Hiroshi Kaneko for useful discussions. This research was partially supported by Nippon Telegraph and Telephone Co., and also by NASA under Grant NAGW-1175.

REFERENCES

1. K. Arakawa and E. Krotkov. *Estimating Fractal Dimension from Range Images of Natural Terrain*, Technical Report CMU-CS-91-156, School of Computer Science, Carnegie Mellon University, Pittsburgh, July 1991.
2. K. Arakawa and E. Krotkov. *Fractal Surface Reconstruction with Uncertainty Estimation: Modeling Natural Terrain*. Technical Report

- CMU-CS-92-194, School of Computer Science, Carnegie Mellon University, Pittsburgh, Oct. 1992.
3. M. Barnsley, Fractal interpolation functions, *Constr. Approx.* **2**, 1986, 303–329.
4. A. Blake and A. Zisserman, *Visual Reconstruction*, MIT Press, Cambridge, MA, 1987.
5. T. Boulton, *Information-Based Complexity in Non-Linear Equations and Computer Vision*, Ph.D. thesis, Department of Computer Science, Columbia University, 1986.
6. L. T. Bruton and N. R. Bartley, Simulation of fractal multidimensional images, using multidimensional recursive filters, *IEEE Trans. on Circuits and Systems-II: Analog and Digital Signal Processing*, **41**(3), 1994, 181–188.
7. P. Burrough, Fractal dimensions of landscapes and other environmental data, *Nature*, **294**, 1981, 240–242.
8. P. Burt, Moment images, polynomial fit filters, and the problem of surface interpolation, in *Proceedings, IEEE Conf. Computer Vision and Pattern Recognition*, Ann Arbor, MI, June 1988, pp. 144–152.
9. M. Deriche and A. H. Tewfik, Maximum likelihood estimation of the parameters of discrete fractionally differenced Gaussian noise process, *IEEE Trans. on Signal Processing*, **41**(10), 1993, 2977–2989.
10. B. Dubuc, *On Evaluating Fractal Dimension*, Master's thesis, McGill University, April 1988, also available as Technical Report TR-CIM-88-13.
11. B. Dubuc, J. Quiniou, C. Roques-Carmes, C. Tricot, and S. Zucker, Evaluating the fractal dimension of profiles, *Phys. Rev. A*, **39**, 1989, 1500–1512.
12. S. Geman and D. Geman, Stochastic relaxation, Gibbs distributions, and the Bayesian restoration of images, *IEEE Trans. Pattern Anal. Machine Intell.* **6**(6), 1984, 721–741.
13. W. E. L. Crimson, *From Images to Surface: A Computational Study of the Human Early Vision System*, MIT Press, Cambridge, MA, 1981.
14. L. M. Kaplan and C.-C. J. Kuo, Texture roughness analysis and synthesis via extended self-similar (ESS) model, *IEEE Trans. Pattern Anal. Machine Intell.* **17**(11), 1995, 1043–1056.
15. J. Keller, S. Chen, and R. Crownover, Texture description and segmentation through fractal geometry, *Comput. Vision Graphics Image Process.* **45**, 1989, 150–166.
16. J. Keller, R. Crownover, and R. Chen, Characteristics of natural scenes related to the fractal dimension, *IEEE Trans. Pattern Anal. Machine Intell.* **9**(5), 1987, 621–627.
17. Y. Kurozumi and W. Davis, Polygonal approximation by the minimax method, *Comput. Graphics Image Process.* **19**, 1982, 248–264.
18. I. Kweon, R. Hoffman, and E. Krotkov, *Experimental Characterization of the Perceptron Laser Rangefinder*, Technical Report CMU-RI-TR-91-1, Robotics Institute, Carnegie Mellon University, Pittsburgh, January 1991.
19. T. Lundahl, W. J. Ohley, S. M. Kay, and R. Siffert, Fractional Brownian motion: A maximum likelihood estimator and its application to image texture, *IEEE Trans. Med. Imaging* **5**(3), 1986, 152–161.
20. B. Mandelbrot, *Fractals, Form, Chance, and Dimension*, Freeman, San Francisco, 1977.
21. B. Mandelbrot, *The Fractal Geometry of Nature*, Freeman, San Francisco, 1982.
22. B. Mandelbrot and J. Van Ness, Fractional Brownian motion, fractional noises and applications, *SIAM REV.* **10**(4), 1968, 422–437.
23. P. Maragos and F.-L. Sun, Measuring the fractal dimension of signals: Morphological covers and iterative optimization, *IEEE Trans. Signal Process.* **41**, 1993, 108–121.
24. J. L. Marroquin, Surface reconstruction preserving discontinuities, A.I. Memo 792, Massachusetts Institute of Technology, August 1984.
25. S. Peleg, J. Naor, R. Hartley, and D. Avnir, Multiple resolution texture analysis and classification, *IEEE Trans. Pattern Anal. Machine Intell.* **6**(4), 1984, 518–523.
26. A. Pentland, Fractal-based description of natural scenes, *IEEE Trans. Pattern Anal. Machine Intell.* **6**(6), 1984, 661–674.
27. T. Poggio, V. Torre, and C. Koch, Computational vision and regularization theory, *Nature* **317**(6035), 1985, 314–319.
28. D. Saupe, Algorithms for random fractals, in *The Science of Fractal Images* (H.-O. Peitgen and D. Saupe, Eds.), Springer-Verlag, Berlin/New York, 1988.
29. R. Stevenson and E. Delp, Viewpoint invariant recovery of visual surfaces from sparse data, *IEEE Trans. Pattern Anal. Machine Intell.* **14**(9), 1992, 897–909.
30. M. A. Stoksik, R. G. Lane, and D. T. Nguyen, Practical synthesis of accurate fractal images, *Graphical Models Image Process.* **57**, 1995, 206–219.
31. R. Szeliski, Regularization uses fractal priors, in *Proc. AAAI-87: Sixth National Conf. Artificial Intelligence*, 1987.
32. R. Szeliski, *Bayesian Modeling of Uncertainty in Low-Level Vision*, Kluwer Academic, Dordrecht/Norwell, MA, 1989.
33. D. Terzopoulos, *Multiresolution Computation of Visible-Surface Representations*, Ph.D. thesis, Massachusetts Institute of Technology, January 1984.
34. D. Terzopoulos, *Computing Visible-Surface Representations*, Technical Report A.I. Memo No. 800, Artificial Intelligence Laboratory, Massachusetts Institute of Technology, Cambridge, MA, March 1985.
35. D. Terzopoulos, Regularization of inverse visual problems involving discontinuities, *IEEE Trans. Pattern Anal. Machine Intell.* **8**(4), 1986, 413–424.
36. R. Voss, Fractals in nature: Characterization, measurement, and simulation, in *The Science of Fractal Images*, (H.-O. Peitgen and D. Saupe, Eds.), Springer-Verlag, Berlin/New York, 1988.
37. G. W. Wornell, Wavelet-based representations for the 1/f family of fractal processes, *Proceedings of the IEEE*, **81**(10), 1993, 1428–1450.
38. N. Yokoya, K. Yamamoto, and N. Funakubo, *Fractal-Based Analysis and Interpolation of 3D Natural Surface Shapes and Their Application to Terrain Modeling*, Technical Report MRCIM-TR-CIM 87-9, McGill University, Montreal, Quebec, July 1987.
39. N. Yokoya, K. Yamamoto, and N. Funakubo, Fractal-based analysis and interpolation of 3D natural surface shapes and their application to terrain modeling, *Comput. Vision Graphics Image Process.* **46**, 1989, 284–302.
40. C. Yoshikawa and E. Krotkov, Parallel fractal interpolation, Submitted to the Worldwide MasPar Challenge, May 1994.